

Thermal Storage and Transport Properties of Rocks, II: Thermal Conductivity and Diffusivity

Encyclopedia of Solid Earth Geophysics

Harsh Gupta (ed.)

Springer

Dr. Christoph Clauser

Professor for Applied Geophysics and Geothermal Energy

E.ON Energy Research Center, RWTH Aachen University

Mathieustr. 6, 52074 Aachen, Germany.

E-mail: cclauser@eonerc.rwth-aachen.de; URL: www.eonerc.rwth-aachen.de/gge

Tel: +49 241-80 49880 ; Fax: +49 241-80 49889

THERMAL STORAGE AND TRANSPORT PROPERTIES OF ROCKS, II: THERMAL CONDUCTIVITY AND DIFFUSIVITY

Synonyms

Thermal conductivity, thermal diffusivity

Definition

Thermal conductivity (also: heat conductivity) λ . Physical property governing heat diffusion in the steady state. It defines how much heat flows across a unit cross-section of rock along a unit distance per unit temperature decrease per unit time; dimension: $\text{W m}^{-1} \text{K}^{-1}$.

Thermal diffusivity κ . Physical property governing transient heat diffusion. It is defined by the ratio of thermal conductivity and thermal capacity, i. e. by the ratio of heat flowing across the face of a unit volume and the heat stored in the unit volume per unit time; dimension: $\text{m}^2 \text{s}^{-1}$.

Thermal conductivity

Fourier's law of heat conduction defines the vector of specific heat flow q_i , i.e. heat flow normalized by area, as the product of the thermal conductivity tensor λ_{ij} and the temperature gradient vector $\partial T/\partial x_j$:

$$q_i = -\lambda_{ij} \frac{\partial T}{\partial x_j}. \quad (1)$$

Temperature measurements are usually performed along vertical profiles in boreholes, yielding only the vertical component of the temperature gradient. Thermal conductivity in some rocks is, to a good approximation, isotropic, particularly in volcanic and plutonic rocks. Then heat will flow predominantly vertically, and it is sufficient to consider only the vertical component of eq. (1). In contrast, thermal conductivity of many sedimentary and metamorphic rocks, is strongly anisotropic, and lateral heat flow may be significant. Hence, information on anisotropy is often required, demanding laboratory measurements in different directions. Anisotropy occurs over a wide range of scales, from microscopic, over laboratory and macroscopic, to tectonic.

Heat transport in most of the Earth's crust and mantle is diffusive and caused by (i) scattering of quantized lattice vibrations, the phonons, and (ii) by diffusive (as opposed to ballistic) radiation of photons. These two processes are described by phonon thermal conductivity λ_p and radiative thermal conductivity, λ_r , respectively, the sum of which is often termed effective thermal conductivity, λ_{eff} . In most polycrystalline material heat radiation starts to dominate at temperatures above 2500 K. In single crystals and glasses with little or no scattering (e. g. obsidian), however, radiation may become important at much lower temperatures of 500 K – 1000 K. In the metallic core, scattering of electrons provides a third heat transfer mechanism (Fig. 1).

Fig. 1 goes here

Fig. 1 Different types of material in the Earth and associated mechanisms of heat

transport (redrawn after Hofmeister et al., 2009).

The following text deals mostly with phonon thermal conductivity. Radiative heat transfer is discussed in the paragraph on radiative thermal conductivity and in the chapter on thermal diffusivity.

Measuring techniques

Thermal conductivity can be measured in the laboratory on rock samples, i. e. cores or cuttings or in situ either in boreholes or with shallow penetration (3 m – 20 m) marine heat flow probes. There are numerous steady-state and transient techniques available for measuring thermal conductivity, the most prominent being the "divided bar", "needle probe", "optical scanning", and "(laser) flash", all of which are suitable to determine also the anisotropy of thermal conductivity. These methods are described in, for instance, Parker et al. (1961); Kappelmeyer & Haenel (1974); Beck (1988); Davis (1988); Somerton (1992); Schilling (1999); Popov et al. (1999b), Beardsmore & Cull (2001); Blumm & Lemarchand (2002). Among these techniques, the transient ones are also suitable for determining thermal diffusivity.

As with most other petrophysical properties, in situ thermal conductivity may deviate significantly from laboratory values, even if the effects of temperature, pressure, and pore fluid are accounted for. This scale dependence involves different aspects: In situ measurements represent an average over a much larger rock volume than laboratory measurements performed on small samples, and cannot resolve small-scale variations. A subsequent upscaling may be necessary to identify the appropriate representative elementary volume (REV) for which reasonable transport parameters averages can be defined.

Indirect methods

When no data are available or no direct measurements can be performed, thermal conductivity can be inferred indirectly, either from mineralogical composition and saturating fluids or from correlations with other physical properties. While some of these methods are based on well defined physical models, others are purely empirical.

Estimation from mineralogical composition and saturating fluids: Thermal conductivity of rocks may be estimated from their mineral and fluid content. Thermal conductivity of minerals vary much less in than rocks, due to their well defined composition. As the bulk thermal conductivity of porous rocks varies with different saturants, it may be also of interest to know rock thermal conductivity for other saturants than those used in the laboratory measurement. Numerous models based on volume fractions of the individual mineral and fluid phases have been proposed, all with specific advantages and disadvantages: Some overestimate while others underestimate systematically the true bulk thermal conductivity. Most of them are valid only within a specific range of volume fractions (or porosities) and yield unreasonable results outside. To overcome this problem, additional parameters may be introduced in order to incorporate rock structure into a mixing law (see below).

The parallel and series models for thermal resistance of layered media are easy to understand, but have the disadvantage of being rather special cases, applicable mostly to bedded sediments. They correspond to the well known weighted arithmetic and harmonic means, λ_{ari} and λ_{har} , eqs. (2)a and (2)b, and are related to heat flowing parallel or perpendicular to bedding, respectively. They define upper and lower limits for all other models, sometimes also referred to as the Voigt upper bound and Reuss lower bound, respectively. Thus they constrain the

maximum variance of possible predictions. The arithmetic mean between the two is known as the Voigt-Reuss-Hill average, λ_{VRH} (eq. (2)c). It is useful for estimating an effective thermal conductivity, while the arithmetic and harmonic means are used to define a range for possible values.

The weighted geometric and square root means λ_{geo} and λ_{sqr} (eqs. (2)d and (2)e; e. g. Beardsmore & Cull, 2001), respectively, are associated with a mixture of different fluid and mineral phases of unspecified geometry. In many cases, both means successfully explain the data and are therefore widely used for lack of more specific information on the geometric arrangement of the individual volume fractions. In the special case where $N=2$ and $n_1 = n_2 = 0.5$, the arithmetic, harmonic, and geometric means are related by $\lambda_{\text{geo}} = \sqrt{\lambda_{\text{ari}} \lambda_{\text{har}}}$.

Effective medium theory (Bruggeman, 1935) provides the effective medium mean λ_{eff} (eq. (2) f) which is useful for macroscopically homogeneous and isotropic rocks consisting of randomly distributed grains and pores.

The upper and lower Hashin-Shtrikman bounds $\lambda_{\text{HS}}^{\text{U}}$ and $\lambda_{\text{HS}}^{\text{L}}$ (eq. (3), Hashin & Shtrikman, 1962), respectively, provide tighter constraints for the predictions of different models other than the arithmetic and harmonic means. The arithmetic average of both defines the Hashin-Shtrikman mean (eq. (2)g). Geometrically, the lower Hashin-Shtrikman bound $\lambda_{\text{HS}}^{\text{L}}$ corresponds to a rock model consisting of grains suspended in a fluid and is closely followed by the geometric mixing law. In contrast, the square root law, is very close to the upper Hashin-Shtrikman bound $\lambda_{\text{HS}}^{\text{U}}$ and could be related to a well lithified rock with spherical, fluid-filled pores. Fig. 2 illustrates the geometries corresponding to all of these models.

Fig. 2 goes here

Fig. 2 Geometrical arrangement of layers, mineral grains, and pores assumed in different models for calculating mean bulk thermal conductivity of a composite medium: arithmetic (λ_{ari}), harmonic (λ_{har}), geometric (λ_{geo}), square root (λ_{sqr}), Hashin-Shtrikman upper ($\lambda_{\text{HS}}^{\text{U}}$) and lower ($\lambda_{\text{HS}}^{\text{L}}$) bounds, and effective medium (λ_{eff}).

If λ_i denotes the thermal conductivity and n_i the volume fraction of the i^{th} phase relative to the total volume ($1=\sum n_i$) these seven weighted means are defined by:

$$\begin{aligned} \text{(a)} \quad \lambda_{\text{max}} = \lambda_{\text{ari}} = \lambda_{\parallel} = \sum_{i=1}^N n_i \lambda_i; \quad \text{(b)} \quad \lambda_{\text{min}} = \lambda_{\text{har}} = \lambda_{\perp} = \left(\sum_{i=1}^N \frac{n_i}{\lambda_i} \right)^{-1}; \quad \text{(c)} \quad \lambda_{\text{VRH}} = \frac{1}{2} (\lambda_{\parallel} + \lambda_{\perp}); \\ \text{(d)} \quad \lambda_{\text{geo}} = \prod_{i=1}^N \lambda_i^{n_i}; \quad \text{(e)} \quad \sqrt{\lambda_{\text{sqr}}} = \sum_{i=1}^N n_i \sqrt{\lambda_i}; \quad \text{(f)} \quad \lambda_{\text{eff}}^{-1} = \sum_{i=1}^N \frac{3 n_i}{2 \lambda + \lambda_i}; \quad \text{(g)} \quad \lambda_{\text{HS}} = \frac{1}{2} (\lambda_{\text{HS}}^{\text{U}} + \lambda_{\text{HS}}^{\text{L}}); \end{aligned} \quad (2)$$

where:

$$\begin{aligned}
\lambda_{\text{HS}}^{\text{U}} &= \lambda_{\text{max}} + \frac{A_{\text{max}}}{1 - \alpha_{\text{max}} A_{\text{max}}}, \\
\text{with: } A_{\text{max}} &= \sum_{i=1; \lambda_i \neq \lambda_{\text{max}}}^N \frac{n_i}{\alpha_{\text{max}} + 1/(\lambda_i - \lambda_{\text{max}})}; \quad \lambda_{\text{max}} = \max(\lambda_1, \dots, \lambda_N); \quad \alpha_{\text{max}} = \frac{1}{3\lambda_{\text{max}}} \\
\lambda_{\text{HS}}^{\text{L}} &= \lambda_{\text{min}} + \frac{A_{\text{min}}}{1 - \alpha_{\text{min}} A_{\text{min}}}, \\
\text{with: } A_{\text{min}} &= \sum_{i=1; \lambda_i \neq \lambda_{\text{min}}}^N \frac{n_i}{\alpha_{\text{min}} + 1/(\lambda_i - \lambda_{\text{min}})}; \quad \lambda_{\text{min}} = \min(\lambda_1, \dots, \lambda_N); \quad \alpha_{\text{min}} = \frac{1}{3\lambda_{\text{min}}}.
\end{aligned} \tag{3}$$

For a two-component system consisting of pore fluid and solid rock with thermal conductivities λ_f and λ_s , respectively, eq. (3) simplifies to (Hashin & Shtrikman, 1962; Horai, 1971):

$$\lambda_{\text{HS}}^{\text{U}} = \lambda_s + \frac{\phi}{\frac{1}{\lambda_f - \lambda_s} + \frac{1 - \phi}{3\lambda_s}}; \quad \lambda_{\text{HS}}^{\text{L}} = \lambda_f + \frac{1 - \phi}{\frac{1}{\lambda_s - \lambda_f} + \frac{\phi}{3\lambda_f}}. \tag{4}$$

Generally, for a two-component system consisting of pore fluid and solid rock with thermal conductivities λ_f and λ_s , respectively, the implicit definition of λ_{eff} in eq. (2)f can be resolved:

$$\begin{aligned}
\lambda_{\text{eff}} &= \frac{1}{4} \left\{ 3\phi(\lambda_f - \lambda_s) + 2\lambda_s - \lambda_f \right. \\
&\quad \left. + \sqrt{9\phi^2\lambda_s^2 + 18\phi\lambda_s\lambda_f - 18\phi^2\lambda_s\lambda_f - 12\phi\lambda_s^2 + \lambda_f^2 - 6\phi\lambda_f^2 + 4\lambda_s\lambda_f + 9\phi^2\lambda_f^2 + 4\lambda_s^2} \right\}.
\end{aligned} \tag{5}$$

Fig. 3 compares the variation of thermal conductivity of a two component system with volume fraction for these different mixing laws defined by eqs. (2) – (5). By and large, and in particular for such a two-component system, thermal conductivity of a multi-phase rock determined according to these models can be ordered as:

$$\lambda_{\perp} = \lambda_{\text{har}} < \lambda_{\text{HS}}^{\text{L}} < \lambda_{\text{VRH}} < \lambda_{\text{geo}} < \lambda_{\text{HS}} < \lambda_{\text{eff}} < \lambda_{\text{sqr}} < \lambda_{\text{HS}}^{\text{U}} < \lambda_{\text{ari}} = \lambda_{\parallel}. \tag{6}$$

Fig. 3 goes here

Fig. 3 Variation of thermal conductivity λ of a two-phase rock with porosity ϕ according to the means in eqs. (2) – (5) for solid and fluid thermal conductivities of $\lambda_{\text{solid}} = 6 \text{ W m}^{-1} \text{ K}^{-1}$ and $\lambda_{\text{fluid}} = 0.6 \text{ W m}^{-1} \text{ K}^{-1}$, respectively: arithmetic (λ_{ari}); Hashin-Shtrikman upper bound ($\lambda_{\text{HS}}^{\text{U}}$); square root (λ_{sqr}); effective medium (λ_{eff}); Hashin-Shtrikman (λ_{HS}); geometric (λ_{geo}); Voigt-Reuss-Hill average (λ_{VRH}); Hashin-Shtrikman lower bound ($\lambda_{\text{HS}}^{\text{L}}$); harmonic (λ_{har}).

While only these nine models are presented and discussed here, various other mixing models are available which take into account additional factors, such as the shape of grains and voids. Several models assume spheroidal pores specifying the aspect ratio of the spheroids (Korvin, 1978, 1982; Schulz, 1981; Zimmerman, 1984, 1989; Buntebarth & Schopper, 1998; Popov et al., 2003). These models require information on the geometry of the internal rock structure and differ in the way of averaging over a representative elementary volume. Horai (1991) tested the results of predictions from several different mixing-models on a remarkable data set in which porosity virtually varies from 0 % – 100 %. As can be expected, most of the models tested were valid only for certain porosity ranges. Only the two-phase models of Fricke-Zimmerman (Fricke, 1924; Zimmerman, 1989) and Schulz (1981) treating pores as spheroidal

inclusions in a homogeneous and isotropic material are valid over the entire range of porosity. However, they require additional information on the spheroids' aspect ratio or orientation. Given the typical ratios of rock and fluid conductivities we observe in nature, i.e. less than 10, most of the conductivity models tested work to within an accuracy of 10 % – 15 %.

Based on 1325 individual measurements on sedimentary rocks and oceanic basalts in dry and saturated condition ($\lambda_{\text{dry}}, \lambda_{\text{sat}}$), Fig. 4 compares the variation of the ratio $\lambda_{\text{dry}}/\lambda_{\text{sat}}$ with porosity measured with that predicted by the arithmetic, upper Hashin-Shtrikman, square root, geometric, lower Hashin-Shtrikman, and harmonic mixing laws, $\lambda_{\text{ari}}, \lambda_{\text{HS}}^{\text{U}}, \lambda_{\text{sqr}}, \lambda_{\text{geo}}, \lambda_{\text{HS}}^{\text{L}},$ and λ_{har} , respectively (eqs. (2) – (4)). It is evident that no single mixing law applies equally well to all rock types. But it appears that the geometric and square root model, on average, provide the best general fits to the data. It is also clear that the upper and lower Hashin-Shtrikman means, $\lambda_{\text{HS}}^{\text{L}}$ and $\lambda_{\text{HS}}^{\text{U}}$ provide much tighter bounds than the arithmetic and harmonic means, λ_{ari} and λ_{har} , respectively.

Fig. 4 goes here

Fig. 4 Variation of thermal conductivity ratio $\lambda_{\text{dry}}/\lambda_{\text{sat}}$ (measured in dry and saturated condition) with porosity ϕ for different rock types. Numbered open circles represent means based on measurements on 1058 sedimentary rock samples (Kobolev et al., 1990; Popov et al., 1995; 1999a; see also Clauser, 2006): (1) 21 limestones; (2) 54 lime-stones; (3) 13 quartz sandstones; (4) 44 quartz silt-stones; (5) 35 conglomerates; (6) 141 quartz sandstones; (7) 33 claystones; (8) 99 polymictic sandstones; (9) 30 quartz sandstones; (10) 22 claystones; (11) 65 quartz silt-stones; (12) 99 quartz silt-stones; (13) 241 quartz silt-stones. Shown for comparison are data measured on 58 oceanic basalts (diamonds) and 179 shaly and limy sandstones (crosses). Curves labeled arithmetic, HS⁺, square root, geometric, HS⁻, and harmonic, correspond to the arithmetic, upper Hashin-Shtrikman, square root, geometric, lower Hashin-Shtrikman, and harmonic mixing laws, $\lambda_{\text{ari}}, \lambda_{\text{HS}}^{\text{U}}, \lambda_{\text{sqr}}, \lambda_{\text{geo}}, \lambda_{\text{HS}}^{\text{L}},$ and λ_{har} , respectively (eqs. (27) – (29)) (Clauser, 2006).

Correlations with other physical properties: Physical properties measured in well-logs can be used to infer estimates for in situ thermal conductivity. The approach is based on an extension of the mixing-model approach to the borehole scale: The volume fractions n_i of the N different mineral (or fluid) phases are either taken directly from induced gamma ray spectroscopy logs (Williams & Anderson, 1990) or determined from a joint analysis of a suitable number J of geophysical logs, such as gamma ray (GR), sonic slowness (DT, the inverse of velocity), gamma density (DEN), and neutron porosity (NPHI) (e. g. Hartmann et al., 2005, Goutorbe et al., 2006). Let \mathbf{x} and \mathbf{b} be vectors composed of the N volume fractions n_i and the J theoretical log responses R^j with respect to the N different phases, respectively. Then, each element R^j of vector \mathbf{b} is the cumulative response of the j^{th} log to all phases weighted by their volume fractions:

$$R^j = \sum_i^N n_i R_i^j, \text{ where: } \sum_i^N n_i = 1, \text{ and } \mathbf{x} = [n_1, \dots, n_N]^T, \mathbf{b} = [R^1, \dots, R^J]^T. \quad (7)$$

The rows of matrix \mathbf{A} contain the specific responses of each log to the N rock phases:

$$\mathbf{A} = \begin{bmatrix} R_1^1 & \cdots & R_N^1 \\ \vdots & \ddots & \vdots \\ R_1^J & \cdots & R_N^J \end{bmatrix}, \quad (8)$$

and the direct and inverse problems can then be written as

$$\mathbf{A} \mathbf{x} = \mathbf{b} \quad \text{and} \quad \mathbf{x} = \mathbf{A}^{-1} \mathbf{b}, \quad (9)$$

respectively. Thus, in the direct problem, the log response vector \mathbf{b} is computed from the volume fraction vector \mathbf{x} and the specific log response matrix \mathbf{A} . In contrast, in the inverse problem, the volume fractions \mathbf{x} are computed from the log responses \mathbf{b} and the inverse of the specific log response matrix, \mathbf{A}^{-1} . Thus, for N solid rock constituents, solving the inverse requires $N-1$ logs. Porosity does not count here, because it follows as the difference of one and the sum of the solid rock volume fractions. If more logs are available, making the problem over-determined, the inverse problem can also be solved in a least-squares sense. Once the volume fractions are known and assigned appropriate thermal conductivities, an appropriate mixing model can be applied to compute rock thermal conductivity. Generally, the geometric and square root means, eqs. (2)d and (2)e, often have turned out useful, but other mixing models may be appropriate in specific cases.

Assigning representative thermal conductivities to the solid rock constituents is not trivial. Tabulated values of rock thermal conductivity should be used only if they characterize specimens from the logged formations. In all other cases, these formations or their outcrops need to be sampled and these specimens tested in the laboratory. If measurements are performed at ambient conditions the values need to be corrected for the effect of temperature, and in some cases for pressure as well.

In general, the effect of temperature is more pronounced than that of pressure. However, for greater depth and little or less consolidated rocks it also needs to be accounted for. If commercial log interpretation software is used to perform the inversion, the theoretical log responses R_i^j with respect to the different rock constituents are usually supplied by the software. Alternatively, values for the theoretical log responses R^j can be obtained from the literature (e. g. Crain, 1986).

Thermal conductivity of minerals and rocks

Thermal conductivity of minerals is much better constrained than that of rocks, due to the well defined crystal structure and chemical formula for each mineral. Substantial collections of mineral thermal conductivities were compiled by Birch (1942), Clark (1966), Horai & Simmons (1969), Dreyer (1974); Roy et al. (1981), Čermák & Rybach (1982), Carmichael (1984), Popov et al. (1987), Diment & Pratt (1988); Somerton (1992), Clauser & Huenges (1995), and Clauser (2006).

Rocks are less well defined. In fact, rock type is a rather poor descriptor for physical properties as it rarely characterizes the dominating factors for any given property. With respect to thermal conductivity, these comprise mineral content, porosity, pore fluid, saturation, and anisotropy for each rock type. As these factors are variable for each rock, the variation of rock thermal conductivity was characterized in a statistical manner in Clauser (2006; 2009) according to the four main diagenetic classes of rocks: sedimentary, volcanic, plutonic and metamorphic. This discussion is summarized here.

Fig. 5 (a - d) goes here

Fig. 5 Histograms of thermal conductivity for (a) sedimentary, (b) volcanic, (c) plutonic, and (d) metamorphic rocks (Clauser, 2009).

For *sedimentary rocks* (Fig. 5a), thermal conductivity is mainly controlled by porosity and sediment type. For *volcanic rocks* (Fig. 5b), porosity is the controlling factor on thermal conductivity: Both mean and median of the high and low porosity histograms differ by nearly a factor of two, and the high-porosity distribution is skewed towards low conductivities. Plutonic and metamorphic rocks are generally much less porous. Here, the controlling factor is the dominant mineral phase. For *plutonic rocks* (Fig. 5c), the feldspar content determines the shape of the histogram: Rocks with a high feldspar content (i. e. > 60 %) display a nearly symmetrical conductivity distribution about a lower mean conductivity than rocks with low feldspar content. In spite of these differences, the means and medians for both distributions are nearly identical. For *metamorphic rocks* (Fig. 5d), it is the quartz content which controls thermal conductivity: Both mean and median of the distributions for high and low quartz content, differ by nearly a factor of two, similar as for *volcanic rocks* (Fig. 5b) with regard to porosity, While the histogram for high quartz content rocks (mostly quartzites) is nearly symmetrical, the low quartz content histogram is strongly skewed towards low conductivities.

Radiative thermal conductivity

In addition to heat conduction, heat radiation emitted from hot bodies propagates through a sufficiently transparent and little absorbing medium as electromagnetic waves with velocity

$$c_m = c_0 / n = \Lambda_m \nu_m, \quad (10)$$

where Λ_m and ν_m are radiation frequency and wavelength in the medium, and $n = c_0 / c_m$ is the ratio of the speed of light in vacuum and in the medium, i. e., the real part of the index of refraction (Tab. 1).

Tab. 1 Refractive index n of selected substances.

Substance	$n = c_0/c_m$ (at 589 nm)	Substance	$n = c_0/c_m$ (at 589 nm)
air	1.0003	zircon ($ZrSiO_4$)	1.92
water(H_2O)	1.33	sulfur (S)	2.00
magnesium fluoride (MgF_2)	1.38	zinc sulfide (ZnS)	2.37
calcium fluoride (CaF_2)	1.43	diamond	2.42
rock salt ($NaCl$)	1.54	carborundum (SiC)	2.55
quartz (SiO_2)	1.54	rutile (TiO_2)	3.10
glass	1.5 – 1.6	galena (PbS) (@ 590 nm)	3,90
carbon disulfide (CS_2)	1.63		
corundum (Al_2O_3)	1.76		

Radiation theory is based on Planck's distribution law defining the spectral radiance L_Λ or L_ν of a black body in the wavelength or frequency interval $d\Lambda_m$ or $d\nu_m$ in the medium in terms of the corresponding wavelength or frequency in vacuum, respectively:

$$L_\Lambda(\Lambda_m, T) d\Lambda_m = \frac{2h c_0^2 n^2(\Lambda, T)}{\Lambda^5 (e^{hc_0/(\Lambda kT)} - 1)} d\Lambda \quad (W m^{-2} sr^{-1} m^{-1} = W m^{-3} sr^{-1}), \quad (11)$$

$$L_\nu(\nu_m, T) d\nu_m = \frac{2h \nu^3 n^2(\nu, T)}{c_0^2 (e^{h\nu/(kT)} - 1)} d\nu \quad (W m^{-2} sr^{-1} Hz^{-1} = W s m^{-2} sr^{-1}),$$

where, $h = 6.626\ 068\ 96(33) \times 10^{-34}$ J s is the Planck constant, $k = 1.380\ 6504(24) \times 10^{-23}$ J K⁻¹ the Boltzmann constant, and $d\Lambda = n d\Lambda_m$. Radiance is the radiant energy flux emitted per unit

solid angle in a given direction per unit projected area of a source. According to Wien's displacement law, the maximum of spectral radiance increases with temperature and decreases with wavelength (or increases with frequency) of radiation. Hofmeister (2005) estimated the variation of $n(\nu, T)$ with temperature and frequency and found both to be very small suggesting that n is approximately constant in the visible frequency range.

The intensity of radiation, I , is related to the incident intensity I_0 , radiation path, x , and opacity, ε , by $I = I_0 \exp(-\varepsilon x)$, where opacity $\varepsilon = 1/l$ is the reciprocal mean free path l of radiation. It defines the average travel distance of photons before being absorbed or scattered. In general, opacity is a function of the radiation wavelength. Opacity in an absorbing and scattering medium comprises contributions from both of these processes:

$$\varepsilon = \alpha + \zeta, \quad (12)$$

where α and ζ are absorption and scattering coefficients, respectively. The scattering coefficient ζ is usually identified with the inverse grain size, suggesting orders of magnitude ranging from 10^2 m^{-1} to 10^6 m^{-1} . The absorption coefficient α may be as large as $\alpha = 7000 \text{ m}^{-1}$, but values below $\alpha = 1500 \text{ m}^{-1}$ are reported for absorption coefficients in single crystal olivines with different proportions of forsterite (Mg_2SiO_4) and fayalite ($\text{Fe}_2^{2+}\text{SiO}_4$) ($\text{Fo}_{94}\text{Fa}_6 - \text{Fo}_{86}\text{Fa}_{14}$) in the two pass bands at $0.5 \mu\text{m}$ and $0.5 \mu\text{m} - 6.0 \mu\text{m}$ (e. g. Shankland et al., 1979; Clauser, 1988; Hofmeister, 2005). The width and level of these pass bands depend critically on the iron content in the minerals. The complex index of refraction of all materials, m , is defined by $m = \sqrt{\varepsilon_r \mu_r} = n - ik$, where ε_r and μ_r are (complex) relative electrical permittivity and relative magnetic permeability, respectively, $n = c_0 / c_m$ is the real and k the imaginary part of the index (sometimes also called extinction coefficient), and $i = \sqrt{-1}$ is the imaginary unit. The absorption coefficient α is related to the complex index of refraction k by

$$\alpha = 4 \pi k / \Lambda, \quad (13)$$

where Λ is the radiation wavelength (Aronsson et al., 1970).

Radiation therefore becomes important for rocks with a larger free mean path of radiation corresponding to smaller values of opacity or absorption coefficient and scattering coefficient. This holds in particular at larger wavelength, in the infra-red part of the absorption spectrum's transmission window between about $0.5 \mu\text{m} - 6.0 \mu\text{m}$.

Radiated heat is diffused if photons emitted by mineral grains are scattered or absorbed by neighboring grains. If the mean free path of radiation, l is small compared to the distance to material discontinuities (such as grain boundaries) and for moderate temperature gradients, i. e. no large anisotropy in the intensity of radiation, an effective thermal conductivity

$$\lambda_{\text{eff},ij} = \lambda_{p,ij} + \lambda_{r,ij} \quad (14)$$

replaces λ_{ij} in eq. (1), where $\lambda_{p,ij}$ and $\lambda_{r,ij}$ are phonon and radiative thermal conductivities, respectively.

Rosseland (1930) and Clark (1957) defined the radiative thermal conductivity based on the temperature derivative of the spectral radiance of a blackbody. Following practice in engineering, Hofmeister (2005) accounts in this expression additionally for the emissivity $\eta \leq 1$ of a grainy material by applying the temperature derivative and the subsequent integration to the product of emissivity η and spectral radiance L_ν , yielding

$$\lambda_r = \frac{4\pi}{3} \int_0^\infty \frac{1}{\varepsilon(\nu, T)} \frac{\partial(\eta(\nu, T) L_\nu(\nu, T))}{\partial T} d\nu. \quad (15)$$

Different practical expressions were derived depending on which parameters can be assumed as independent of temperature or frequency (see e. g. Clark (1957); Shankland et al. (1979); Schärmeli, 1982; Clauser, 1988; Hofmeister, 1999, 2005; Hofmeister et al., 2009).

Based on grain size δ and attenuation

$$A = (\ln I_0 - \ln I_t) / \delta \approx \alpha, \quad (16)$$

where α is the absorption coefficient and I_0 and I_t are incident and transmitted intensities, respectively, Hofmeister (2005) suggests the following expressions for emissivity and opacity:

$$\eta = 1 - e^{-\delta\alpha(\nu)} = 1 - e^{-(\ln I_0 - \ln I_t)}, \quad \varepsilon = \frac{1 + \delta\alpha}{\delta}, \quad (17)$$

and estimates values for the product $\delta\alpha$ based on the interface reflectivity R (%) between two neighboring grains. Values for $\delta\alpha$ considered realistic for the mantle range between 5 and 10 (corresponding to a range for R between 0.7 % – 0.05 %) with a preferred value of 7 ($R = 0.1$ %).

The “gray body” approximation assumes opacity and emissivity as finite, constant, and independent of radiation wavelength. If the real part of the refractive index, n , and the spectral radiance, L_Λ or L_ν , are also independent of temperature and wavelength, eq. (15) simplifies into:

$$\lambda_r = \frac{16\eta\sigma n^2 T^3}{3\varepsilon}, \quad (18)$$

where $\sigma = 5.670\,400(40) \times 10^{-8} \text{ W m}^{-2} \text{ K}^{-4}$ is the Stefan-Boltzmann constant. An example of magnitude is obtained when emissivity $\eta = 0.99$ and opacity ε is identified with the olivine ($\text{Fo}_{92}\text{Fa}_8$) absorption coefficient α at 1700 K (eq. (12), neglecting contributions from scattering), with $1000 \text{ m}^{-1} < \alpha < 1500 \text{ m}^{-1}$. Additionally, a typical silicate value is assumed for the index of refraction, $n = 1.6$ (Tab. 1). This yields a range for radiative thermal conductivity at 1700 K of $3.8 \text{ W m}^{-1} \text{ K}^{-1} > \lambda_r > 2.5 \text{ W m}^{-1} \text{ K}^{-1}$.

Inserting eqs. (16), (17), and the temperature derivative of the spectral radiance (11) as provided by Shankland et al. (1979) into (15) yields radiative thermal conductivity as:

$$\begin{aligned} \lambda_r &= \frac{4\pi\delta}{3} \int_0^\infty \frac{1 - e^{-\delta\alpha(\nu)}}{1 + \delta\alpha(\nu)} \frac{\partial(L_\nu(\nu, T))}{\partial T} d\nu \\ &= \frac{8\pi\delta n T^3 k^4}{3c_0^2 h^3} \sum_{\text{lower}}^{\text{upper}} \int \frac{1 - e^{-\delta\alpha(\nu)}}{1 + \delta\alpha(\nu)} \left[\frac{n e^x x^4}{e^x - 1} + \frac{2T x^3}{e^x - 1} \frac{\partial n}{\partial T} \right] dx \quad (\text{W m}^{-1} \text{ K}^{-1}), \end{aligned} \quad (19)$$

where $x = h\nu / (k T)$ and $dx = h d\nu / (k T)$, and the summation allows for the transparent regions above and below the strong absorption bands in the visible part of the spectrum. The second term of the sum in the integrand vanishes if $\partial n / \partial T \approx 0$ as suggested by Hofmeister (2005). Because α varies nonlinearly with frequency or wavelength, and the cut-off frequencies in the integral in (19) depend on δ and α , Hofmeister (2005) evaluated the integral numerically for polynomials in T whose exponents ranged from 0 to 6, thus yielding other than a purely cubic relationship between radiative thermal conductivity and temperature.

Variation with temperature

Since the pioneering experiments of Eucken (1911), thermal conductivity of minerals and rocks is known to decrease with temperature, generally with its inverse. Eucken's empirical result was corroborated theoretically by Peierls (1929) based on Debye's (1914) theory of phonon scattering. Eucken (1911) observed in his experiments in contrast to crystals an increase in thermal conductivity of amorphous siliceous glass, a clear indication of radiative heat transfer.

The decrease is primarily due to the decrease of phonon (or lattice) thermal conductivity λ_p with temperature and to a smaller degree to thermal cracking. Since the thermal expansion coefficient increases with temperature (but differently for all minerals) differential expansion may create contact resistances between mineral grains. The effect of contact resistance is less pronounced in water-saturated than in dry rocks, the condition in which most rocks are tested at elevated temperatures. For single-mineral aggregates, a linear relationship between temperature and thermal resistivity, λ^{-1} , discriminates between contributions which depend on temperature T and others which don't, such as micro-cracks, grain boundaries, shape and orientation of crystals and their fragments:

$$\lambda^{-1}(T) = c_1 + c_2 T, \quad (20)$$

where λ is in $\text{W m}^{-1} \text{K}^{-1}$ and T is in K. By measuring thermal conductivity λ and plotting its inverse, thermal resistivity λ^{-1} , versus temperature, constants c_1 and c_2 are obtained from intercept and slope of a linear regression. Tab. 2 provides values for the constants c_1 and c_2 in eq. (20) which may be used to infer the temperature dependence of thermal resistivity for some single-mineral aggregates (Clark, 1969).

Tab. 2 Values of c_1 and c_2 in eq. (20) for single-mineral aggregates; data: Clark (1969).

Mineral	T (°C)	$c_1 \times 10^3$ ($\text{W}^{-1} \text{m K}$)	$c_2 \times 10^3$ ($\text{W}^{-1} \text{m}$)
<i>halite, NaCl</i>	0 - 400	-52.55	0.788
<i>periclase, MgO</i>	100 - 800	-21.50	0.127
<i>corundum, Al₂O₃</i>	100 - 800	-28.66	0.155
<i>quartz, SiO₂ (*)</i>	100 - 400	62.10	0.387
<i>spinel, MgAl₂O₄</i>	100 - 1000	19.11	0.122
<i>Zircon, ZrSiO₄</i>	100 - 800	131.37	0.093
<i>forsterite, Mg₂SiO₄</i>	100 - 600	85.98	0.282
<i>enstatite, ferrosilite, (Mg₂,Fe₂)SiO₃</i>	100 - 300	200.63	0.222

(*): single SiO₂ crystal, heat flowing \perp to optical axis

Based on measurements on 113 samples of metamorphic rocks from the KTB research borehole in Germany in the temperature range 50 °C – 200 °C, Buntebarth (1991) determined mean values for the constants c_1 and c_2 in eq. (20) for gneissic and metabasitic rocks. The arithmetic means determined from measurements on 66 gneiss samples are $\bar{c}_1 = 0.16(3) \text{ W}^{-1} \text{m K}$ and $\bar{c}_2 = 0.37(14) \times 10^{-3} \text{ W}^{-1} \text{m}$. The corresponding means determined from measurements on 36 metabasite samples are $\bar{c}_1 = 0.33(3) \text{ W}^{-1} \text{m K}$ and $\bar{c}_2 = 0.22(14) \times 10^{-3} \text{ W}^{-1} \text{m}$.

In contrast to phonon conductivity λ_p , the radiative contribution to thermal conductivity, λ_r , increases with the cube of temperature (see above). Thus, measurements of thermal conductivity as function of temperature generally first exhibit a decrease with temperature until, from about 1000 °C – 1200 °C onwards, the radiative component balances and sometimes even reverses the decreasing trend.

The temperature dependence of rock thermal conductivity was characterized in a statistical manner in Clauser (2006; 2009) according to the four main diagenetic classes of rocks: sedimentary, volcanic, plutonic and metamorphic. This discussion is summarized here (Fig. 6):

Fig. 6 (a - d) goes here

Fig. 6 Variation of thermal conductivity with temperature for (a) sedimentary, (b) volcanic, (c) plutonic, and (d) metamorphic rocks. Color shading indicates a range defined by plus and minus one standard deviation and N is the number of data at each temperature (Clauser, 2009).

For *sedimentary rocks* (Fig. 6a) up to 300 °C there is a reduction by nearly a factor of two, both for physical and chemical sediments. Above 300 °C, the decrease in thermal conductivity is less, but it is stronger for chemical sediments than for physical sediments. However, there are very few data for this temperature range, which makes this last observation statistically weak. Above 300 °C, the mean thermal conductivity of sediments varies between $1.0 \text{ W m}^{-1} \text{ K}^{-1}$ – $1.5 \text{ W m}^{-1} \text{ K}^{-1}$.

Volcanic rocks (Fig. 6b) vary quite differently with temperature depending on their opacity, i.e. on how well they transmit thermal energy by radiation. Due to this additional "radiative thermal conductivity", volcanic glasses and rocks with small iron content experience an increase in thermal conductivity for temperatures above 800 °C – 1000 °C (e. g. Clauser, 1988; Hofmeister et al., 2009). In contrast, thermal conductivity of conduction dominated rocks, such as rocks with high iron content, decreases with temperature. An inversion of this trend is indicated by few available high-temperature measurements (above 1300 °C) but with too few measurements for a statistical appraisal. At about 1000 °C thermal conductivity for these rocks is at about 50 % of the room-temperature value. Again, there are few data points above 700 °C.

Plutonic rocks (Fig. 6c), show no strong radiative contribution. At temperatures above 600 °C, thermal conductivity decreases only very little. However, in these rocks the variation of thermal conductivity with temperature depends on their feldspar content. For rocks enriched in feldspar, thermal conductivity decreases little up to 300 °C, while for those poor in feldspar the decrease is stronger, becoming more gentle above 300 °C, and spreading an additional 20 % over the next 1000 K. The different behavior of rocks with high feldspar content is due to the increase in thermal conductivity with temperature of some plagioclase feldspars (e. g. Höfer & Schilling, 2002; Petrunin et al., 2004) which compensates the decrease in thermal conductivity with temperature observed for most other minerals and rocks. Other notable exceptions are fused silica as well as volcanic and silica glasses.

For *metamorphic rocks* (Fig. 6d), the decrease of thermal conductivity with temperature depends on the content in a dominant mineral phase, similar as for plutonic rocks. For quartzites, the decrease is strong, by nearly a factor of three up to a temperature of about 500 °C with only a very mild further decrease beyond this temperature. For rocks poor in quartz the decrease in conductivity is not quite as strong, amounting to about one third of the room-temperature value up to 300 °C. Then it remains roughly constant up to 500 °C and decreases again to about one third of the room-temperature value up to 750 °C.

In summary, for moderate temperatures thermal conductivity of rocks is well described by a linear relationship with inverse temperature, similar as in eq. (20). For this temperature range several approaches are available for inferring thermal conductivity at elevated temperatures.

Based on the analysis of available tabulated data of thermal conductivity as function of temperature Zoth & Hänel (1988) suggested the following form:

$$\lambda(T) = A + \frac{B}{350 + T} \quad (0 \text{ } ^\circ\text{C} \leq T \leq 800 \text{ } ^\circ\text{C}), \quad (21)$$

where average values of the coefficients A and B for different rock types are given in Tab. 3:

Tab. 3 Values for constants A and B in eq. (21) for different rock types (Zoth & Hänel, 1988).

Rock Type	T (°C)	A (W m ⁻¹ K ⁻¹)	B (W m ⁻¹)
(1) rock salt	-20 – 0	-2.11	2960
(2) limestones	0 – 500	0.13	1073
(3) metamorphic rocks	0 – 1200	0.75	705
(4) acidic rocks	0 – 1400	0.64	807
(5) basic rocks	50 – 1100	1.18	474
(6) ultra-basic rocks	20 – 1400	0.73	1293
(7) rock types (2)-(5)	0 – 800	0.70	770

Linear relationships between temperature and thermal resistivity, such as eqs. (20) and (21), discriminate between temperature-dependent contributions and other factors, which are independent of temperature, such as micro-cracks, grain boundaries, pore volume, mineralogical composition, shape and orientation of crystals and their fragments.

Tab. 4 Coefficients a, b, and c in eq. (22) and associated uncertainties Δa , and σ_b , σ_c ; Δa is the error of the mean intercept \bar{a} for all rock types of the linear regressions of the normalized thermal resistance $\lambda_0/\lambda(T)$ as a function of temperature T; σ_b and σ_c are the errors defined by the linear regression of the slopes $(b-c/\lambda_0)$ as a function of the thermal resistance $1/\lambda_0$ (see eq. (22)); references: (1) = Sass et al., 1992; (2) = Vosteen & Schellschmidt, 2003.

Rock Type	\bar{a} (-)	Δa (%)	$b \times 10^3$ (K ⁻¹)	$\sigma_b \times 10^3$ (K ⁻¹)	$c \times 10^3$ (W m ⁻¹ K ⁻²)	$\sigma_c \times 10^3$ (W m ⁻¹ K ⁻²)	T (°C)	Reference
Basement Rocks I (from felsic gneiss to amphibolite)	1.007	-	3.6	-	7.2	-	0 – 250	(1)
Basement Rocks II (magmatic and metamorphic)	0.99	1	3.0	1.5	4.2	0.6	0 – 500	(2)
Sediments	0.99	1	3.4	0.6	3.9	1.4	0 – 300	(2)

Sass et al. (1992) and Vosteen & Schellschmidt (2003) distinguish between the effects of composition and temperature. They propose a general empirical relation for $\lambda(T)$, the thermal conductivity in W m⁻¹ K⁻¹ at temperature T in °C, as a function of λ_0 , the thermal conductivity at 0 °C:

$$\lambda(T) = \frac{\lambda_0}{a + T \left(b - \frac{c}{\lambda_0} \right)} \quad \text{or} \quad \frac{\lambda_0}{\lambda(T)} = \underbrace{a}_{\text{intercept}} + \underbrace{\left(b - \frac{c}{\lambda_0} \right)}_{\text{slope}} T \quad (22)$$

For different rock types, the slopes and intercepts of this equation can be determined from linear regressions of eq. (22) yielding a mean intercept \bar{a} and its uncertainty Δa . Coefficients b

and c and associated uncertainties σ_b and σ_c are determined from a second linear regression of the different slopes ($b-c/\lambda_0$) as a function of $1/\lambda_0$ (Tab. 4).

Since thermal conductivity is usually measured at room temperature, λ_0 is expressed as a function of λ_{25} , the room temperature thermal conductivity, by Sass et al. (1992) for crystalline rocks (felsic gneiss to amphibolite) as:

$$\lambda_0 = \lambda_{25} \left(1.007 + 25 \left(0.0037 - \frac{0.0074}{\lambda_{25}} \right) \right). \quad (23)$$

Vosteen & Schellschmidt (2003) find for magmatic and metamorphic rocks:

$$\lambda_0 = 0.53 \lambda_{25} + 0.5 \sqrt{1.13 \lambda_{25}^2 - 0.42 \lambda_{25}}, \quad (24)$$

and for sedimentary rocks:

$$\lambda_0 = 0.54 \lambda_{25} + 0.5 \sqrt{1.16 \lambda_{25}^2 - 0.39 \lambda_{25}}. \quad (25)$$

Hofmeister (1999) provided a detailed analysis of heat transport based on an analysis of phonon lifetimes obtained from infrared reflectivity. It accounts for the variation of the phonon contribution λ_p to thermal conductivity with both temperature and pressure as well as for the pressure dependent radiative contribution λ_r . It allows approximation of thermal conductivity for mantle conditions if: (1) K'_0 , the pressure derivative of the isothermal bulk modulus K_T , is constant: $K'_0 = dK_T / dP = \text{const}$; (2) the variations of the bulk modulus with temperature and pressure are mutually independent; (3) the pressure derivative of the thermodynamic Grüneisen parameter γ (eqs. 12 or 13 in the companion article “Thermal Storage and Transport Properties of Rocks, I: Heat Capacity and Latent Heat” in this volume) is constant: $d\gamma / dP = f$. For mantle material, γ varies from 1 – 1.4, K'_0 from 4 – 5, and $f \approx 0$ vanishes approximately. According to Hofmeister (1999) and within the uncertainty of these parameters, thermal conductivity in the mantle is:

$$\lambda(T, P) = \lambda_{298\text{K}, 101.33\text{kPa}} \times (298/T)^a \left(1 + K'_0 P / K_T \right) e^{-\frac{(4\gamma+1/3)}{298} \int_{298}^T \alpha(T') dT'} + \lambda_r, \quad (26)$$

$K'_0 P / K_T$

where T is absolute temperature, $\lambda_{298\text{K}, 101.33\text{kPa}}$ is thermal conductivity at room temperature and atmospheric pressure, $\alpha(T)$ is volume coefficient of thermal expansion as a function of temperature, and the exponent a is the fitting parameter. The radiative contribution λ_r in (26) may be approximated by eqs. (15), (18), or (19). Hofmeister (1999) provides alternative expressions for λ_r for ferrous minerals or dense silicates and oxides (Fig. 8):

ferrous minerals :

$$\lambda_r = 0.01753 - 1.0365 \times 10^{-4} T + 2.2451 \times 10^{-7} T^2 - 3.407 \times 10^{-11} T^3; \quad (27)$$

dense silicates and oxides

$$\lambda_r = 8.5 \times 10^{-11} T^3 \quad (\lambda_r \text{ in } \text{W m}^{-1} \text{K}^{-1} \text{ and } T \text{ in K}).$$

Fig. 1 in the companion article in this volume (“Thermal Storage and Transport Properties of Rocks, I: Heat Capacity and Latent Heat”) shows the variation of phonon thermal conductivity λ_p with temperature in an average crust of density $\rho = 2700 \text{ kg m}^{-3}$ molar mass of $0.22178 \text{ kg mol}^{-1}$. It is derived from $\lambda = \kappa \rho c$ as the product of thermal capacity ρc_p and thermal diffusivity κ calculated according to eq. 20 (in the companion article in this volume “Thermal Storage and Transport Properties of Rocks, I: Heat Capacity and Latent Heat”; Whittington et al., 2009). Due to the balancing increase of specific heat capacity with temperature, the de-

crease in thermal conductivity with temperature is less than in thermal diffusivity by a factor of about 1.3. Assuming a constant density throughout the crust, this implies that the increase and decrease in density due to the increase in pressure and temperature, respectively, partly cancel each other and that these changes are small compared to those of specific heat capacity and thermal diffusivity.

Fig. 7 goes here

Fig. 7 Variation of radiative thermal conductivity λ_r of ferrous minerals, dense silicates, and oxides with temperature according to eq. (27) (Hofmeister, 1999).

For mantle minerals, such as olivine and its high-pressure polymorphs, the β - and γ -spinel wadsleyite and ringwoodite, respectively, Xu et al. (2004) fitted phonon thermal conductivity measured to 1373 K and 20 GPa to an exponential equation in temperature yielding values for the exponent between -0.406(35) – -0.537(11) suggesting that fitted phonon thermal conductivity varies with $T^{-1/2}$ (Tab. 5).

Tab. 5 Reference values λ_{298} and κ_{298} at 298 K, pressure coefficients a and a' , and fitting functions for thermal conductivity λ and thermal diffusivity κ of lower mantle minerals with absolute temperature T and pressure P (Xu et al., 2004).

Mineral	$\lambda = \lambda_{298} (298/T)^{1/2} (1+aP)$		$\kappa = \kappa_{298} (298/T)^n (1+a'P)$			
	P (GPa)	λ_{298} (W m ⁻¹ K ⁻¹)	a (GPa ⁻¹)	$\kappa_{298} \times 10^6$ (m ² s ⁻¹)	n	a' (GPa ⁻¹)
<i>olivine</i>	4 – 10	4.13(11)	0.032(3)	1.31(5)	0.681(22)	0.036(4)
	4	4.49(4)	–	1.29(5)	0.563(35)	–
	7	5.19(4)	–	1.74(4)	0.720(26)	–
	10	5.56(4)	–	1.84(5)	0.723(31)	–
<i>wadsleyite</i>	14	8.10(4)	0.023	2.55(3)	0.721(13)	–
<i>ringwoodite</i>	20	9.54(5)	0.022	3.09(4)	0.793(17)	–

Variation with pressure

The effect of pressure on phonon thermal conductivity λ_p is different in two distinct pressure ranges. First, fractures and micro-cracks (developed during stress release after sampling) begin to close with increasing pressure. This reduces thermal contact resistance as well as porosity which is usually filled with a low conductivity fluid. This process ends when a pressure of about 15 MPa is reached. A compilation of measurements on various sedimentary, volcanic, plutonic and metamorphic rocks (Clauser & Huenges, 1995) indicates that this effect accounts for an increase of about 20 % relative to thermal conductivity at atmospheric pressure. A further pressure increase to 40 MPa does not affect thermal conductivity significantly. If pressure is increased further, however, a second process becomes effective, the reduction of intrinsic porosity, i.e. voids which are not created by stress release. For granite and for metamorphic rocks, data indicate an increase of thermal conductivity by about 10 % within the pressure range 50 MPa – 500 MPa.

For mantle minerals, such as olivine and its high-pressure polymorphs, the β - and γ -spinel wadsleyite and ringwoodite, respectively, Xu et al. (2004) determined values for the pressure coefficient between 0.022 GPa⁻¹ and 0.032 GPa⁻¹ for phonon thermal conductivity measured

to 1373 K and 20 GPa (Tab. 5). A table of numerical values for pressure derivatives of phonon thermal conductivity measured by a variety of authors was compiled by Hofmeister et al. (2009). Most values for $\lambda^{-1} (\partial\lambda / \partial P)$ fall into the range $0.04 \text{ GPa}^{-1} - 0.36 \text{ GPa}^{-1}$, exceeded only by values of 0.69 GPa^{-1} and 0.5 GPa^{-1} for sulfur and quartz_{⊥c} (measured perpendicular to the optical c-axis), respectively. Osako et al. (2004) fitted thermal conductivity measured to 1100 K and 8.3 GPa on isotropic, single-crystal garnet and anisotropic olivine (Fo₉₃Fa₇; in three crystallographic directions) as upper and lower mantle constituents, respectively, to a linear equation in pressure (Tab. 6). A pressure dependence of garnet and olivine was found on the order of $4 \% \text{ GPa}^{-1} - 5 \% \text{ GPa}^{-1}$ and $3 \% \text{ GPa}^{-1} - 4 \% \text{ GPa}^{-1}$, respectively.

Tab. 6 Coefficients and fitting functions for the variation thermal conductivity λ and thermal diffusivity κ of garnet and olivine with absolute temperature T and pressure P (Osako et al., 2004).

Garnet				Olivine			
$\lambda = C_0 + C_1/T$		$\lambda = A_0 + A_1 P$		$\lambda = C_0 + C_1/T$		$\lambda = B_0 \exp(B_1 P)$	
C_0 (W m ⁻¹ K ⁻¹)	C_1 (W m ⁻¹)	A_0 (W m ⁻¹ K ⁻¹)	A_1 (W m ⁻¹ K ⁻¹ GPa ⁻¹)	C_0 (W m ⁻¹ K ⁻¹)	C_1 (W m ⁻¹)	B_0 (W m ⁻¹ K ⁻¹)	B_1 (GPa ⁻¹)
2.01(8)	704(43)	3.48(33)	0.160(26)	[100] 1.91(28)	2088(163)	6.61(13)	0.038(5)
				[010] 0.84(36)	1377(157)	3.98(15)	0.042(5)
				[001] 2.08(38)	1731(86)	5.91(25)	0.034(5)
$\kappa = c_0 + c_1/T$		$\kappa = a_0 + a_1 P$		$\kappa = c_0 + c_1/T$		$\kappa = b_0 \exp(b_1 P)$	
$c_0 \times 10^6$ (m ² s ⁻¹)	$c_1 \times 10^6$ (m ² s ⁻¹ K)	$a_0 \times 10^6$ (m ² s ⁻¹)	$a_1 \times 10^6$ (m ² s ⁻¹ GPa ⁻¹)	$c_0 \times 10^6$ (m ² s ⁻¹)	$c_1 \times 10^6$ (m ² s ⁻¹ K)	$b_0 \times 10^6$ (m ² s ⁻¹)	b_1 (GPa ⁻¹)
0.29(6)	374(31)	1.19(6)	0.046(1)	[100] -0.06(11)	938(46)	2.50(4)	0.033(5)
				[010] -0.13(8)	626(45)	1.52(6)	0.040(7)
				[001] -0.03(17)	832(98)	2.16(14)	0.035(3)

In contrast, radiative thermal conductivity λ_r was found much less variable with pressure than with temperature (Clark, 1957). In particular, this holds once the spectral radiance overlaps the infrared pass band in the absorption spectrum, at temperatures above 1900 K (Hofmeister, 2005).

Variation with other factors

Apart from temperature and pressure, thermal conductivity also varies with porosity, pore fluid, saturation, dominant mineral phase, and anisotropy. These effects are summarized here from the detailed discussion in Clauser (2006):

For large *porosity* (i. e. $\phi \gg 1 \%$) thermal conductivity of the saturating fluid affects significantly the bulk rock thermal conductivity. The influence varies with the thermal conductivity of the saturants, e. g. water, oil, natural gas, air. The resulting bulk thermal conductivity can be estimated from a suitable mixing model, e. g. eqs. (2) – (4).

The effect of partial *saturation* is different for porous or fractured rocks. In porous rocks, porosity comprises both bulk pore space and bottlenecks formed by the contact between individual grains. Dry bottlenecks act as thermal contact resistances between grains, while the bulk pore volume contributes proportionally to the effective rock thermal conductivity. In fractured rocks, in contrast, there are no bottlenecks between grains as in porous rocks, and the small void volume in the fractures corresponds to the bulk pores space of porous rocks.

Fig. 8 goes here

Fig. 8 Variation of thermal conductivity with partial saturation for a sandstone (circles; $\phi = 18\%$) and granite (squares; $\phi = 1\%$) saturated with water and standard deviations (bars); values normalized by reference thermal conductivities shown in legend (Clauser (2006) based on data of Reibelt (1991)).

Fig. 8 illustrates these two effects for a water-saturated medium-porosity sandstone and a low-porosity granite: Starting completely dry with an unsaturated conductivity of about 60 % of the saturated value, a level of 85 % is reached for the sandstone at about 10 % saturation. The 15 % conductivity residual is then spread almost linearly over the remaining 90 % of saturation. Physically this observation indicates that the filling of inter-granular bottlenecks accounting for only about 10 % – 15 % of the total porosity significantly reduces the contact resistances between the individual grains. In contrast, the replacement of low conductivity air by the more conductive fluid in the major part of the pore volume accounts for the second effect. If only fractures contribute to the total porosity, as in the granite, there are no bottlenecks and only the second effect is observed: Starting completely dry with an unsaturated conductivity of about 85 % of the saturated conductivity a quasi linear increase is observed due to the replacement of low conductivity air until the 100 % level is reached for complete saturation.

Anisotropy of sedimentary and metamorphic rocks is due to the conditions of their formation. Anisotropy exists on several scales: (i) On the microscopic scale, many minerals are anisotropic; (ii) on the laboratory scale, thermal conductivity of many rocks is also anisotropic. However, even if rocks are composed of anisotropic minerals, random orientation of the crystals within the rock may render the rock's bulk thermal conductivity isotropic on a macroscopic scale; (iii) on a still larger scale, if rocks are exposed to folding, orogenic or other tectonic processes, thermal conductivity of the resulting rock formation may be anisotropic.

As a result, thermal conductivity parallel to the direction of layering or foliation, λ_{\parallel} , is greater than thermal conductivity in the perpendicular direction, λ_{\perp} . The factor of anisotropy, the ratio $\lambda_{\parallel} / \lambda_{\perp}$, generally falls into the range 0.9 – 3, with most values between 1 – 2 (e. g. Clauser & Huenges, 1995; Popov & Mandel, 1998; Popov et al., 1999a,b; Clauser, 2006; Davis et al., 2007). For sedimentary rocks a general trend been reported of decreasing λ_{\perp} with factor of anisotropy $\lambda_{\parallel} / \lambda_{\perp}$, but no such trend was identified for metamorphic rocks (Clauser, 2006).

Thermal diffusivity

Thermal diffusivity is required in the analysis of transient heat transfer. A sizable compilation of room-temperature data of phonon thermal diffusivity κ_p measured on various mantle minerals is given by Hofmeister et al. (2009) from measurements by various groups.

If both conductivity and thermal capacity are known, thermal diffusivity κ can be calculated from $\kappa = \lambda / (\rho c)$. As for steady-state thermal conduction, transient heat diffusion in most of the Earth's crust and mantle is caused by scattering of quantized lattice vibrations, the phonons, and by diffusive (as opposed to ballistic) radiation of photons. These two processes are described by phonon thermal conductivity λ_p and radiative thermal conductivity, λ_r , respectively, the sum of which is often termed effective thermal conductivity, λ_{eff} . As thermal diffusivity is the ratio of thermal conductivity and thermal capacity, it is also influenced by the variation of density and specific heat capacity. This is of particular interest with respect to the variation with temperature.

Measuring techniques

All of the transient laboratory methods used to determine thermal conductivity are useful to determine thermal diffusivity as well. Recently, heat pulse (Schilling, 1999; Höfer & Schilling, 2002; Gibert et al., 2003) and laser flash methods (Parker et al., 1961; Blumm & Lemarchand, 2002; Hofmeister, 2006) have been used for measurements at high temperature. Compared to other methods their advantage lies in a reduction or even complete absence of physical contacts between samples on the one hand and temperature sensors and heat sources on the other hand. While most methods measure the effective diffusivity comprising contributions from phonon conduction and diffused heat radiation, the laser flash method yields the diffusive component without contributions from heat radiation. This difference becomes important particularly at high temperatures (for a critical assessment see e.g. Hofmeister et al., 2009).

Variation with temperature

Thermal diffusivity κ of rocks varies even more strongly with temperature than thermal conductivity λ . This is caused by the opposite behavior of thermal conductivity and thermal capacity (ρc) with respect to temperature. Because of several self-compensating factors, thermal capacity (ρc) with few exceptions generally varies within $\pm 20\%$ of $2.3 \text{ MJ m}^{-3} \text{ K}^{-1}$ for the great majority of minerals and rocks (Beck, 1988). This is confirmed by a linear regression of thermal diffusivity on thermal conductivity which was measured on a suite of meta-sedimentary, volcanic, magmatic, and metamorphic rocks together with density and specific heat capacity (Mottaghy et al., 2005):

$$\kappa = \frac{\lambda}{\rho c} = \frac{\lambda}{2.3} = 0.44 \lambda \quad (\kappa \text{ in } 10^{-6} \text{ m}^2 \text{ s}^{-1}). \quad (28)$$

A linear regression of thermal capacity as a function of temperature yields also a linear relationship. This allows to determine thermal diffusivity $\kappa(T)$ at any temperature, based only on the known variation of thermal conductivity $\lambda(T)$ with temperature (Mottaghy et al. (2005):

$$\kappa(T) = \frac{\lambda(T)}{2.134 + 0.0044 T} \quad (\kappa \text{ in } 10^{-6} \text{ m}^2 \text{ s}^{-1}; \quad T \text{ in } ^\circ\text{C}). \quad (29)$$

Thus, thermal diffusivity can be derived from thermal conductivity and vice versa. For the suite of rocks studied by Mottaghy et al. (2005), thermal conductivity decreased by $4\% - 7\%$ in the range $1^\circ\text{C} - 100^\circ\text{C}$ while thermal diffusivity decreased by $18\% - 22\%$.

Thermal diffusivity was measured at temperatures of up to 550°C by Ray et al. (2006) on a suite of 16 samples comprising Archean granulitic rocks which are considered a major component of the middle and lower continental crust. Phonon scattering was found dominating heat transport with radiative diffusion of photons setting in at 450°C for most, but not all rocks. Based on their measurements, Ray et al. (2006) propose an equation by which thermal diffusivity $\kappa(T)$ at elevated temperature below 450°C can be derived from room temperature values, κ_{rt} :

$$\kappa(T) = 0.7 + 144 \frac{\kappa_{rt} - 0.7}{T - 150} \quad (\kappa \text{ in } 10^{-6} \text{ m}^2 \text{ s}^{-1}; \quad T \text{ in K}), \quad (30)$$

They also proposed an additional term in eq. (30), proportional to T^3 , by which the radiative contribution above 450°C is fitted. However, this assumes a similar variation with tempera-

ture of thermal conductivity and thermal diffusivity and neglects the additional variation of specific heat capacity. This, in fact, makes thermal diffusivity vary stronger with temperature than thermal conductivity, which is why the T^3 -term is omitted here. Whittington et al. (2009) measured the phonon component κ_p of thermal diffusivity at temperatures of up to 1 260 K on garnet schist, leucogranite, and welded rhyolitic ash-flow tuff using laser flash analysis. This characterizes purely the phonon heat transfer component without any radiative contribution, in contrast to the values discussed above. Below and above the transition between α - and β -quartz at 846 K (~ 573 °C) the data are reasonably fitted by

$$\kappa_p(T) = \begin{cases} -0.062 + \frac{567.3}{T}; & T < 846 \text{ K} \\ 0.732 - 0.000135 T; & T > 846 \text{ K} \end{cases} \quad (\kappa \text{ in } 10^{-6} \text{ m}^2 \text{ s}^{-1}; T \text{ in K}), \quad (31)$$

assuming an average molar mass of $0.22178 \text{ kg mol}^{-1}$ and an average density of 2700 kg m^{-3} for the crust (see Fig. 1 in the companion article ‘‘Thermal Storage and Transport Properties of Rocks, I: Heat Capacity and Latent Heat’’ in this volume). The leucogranite and rhyolite samples were homogeneous and isotropic. The schist was anisotropic owing to alternating mica- and quartz-rich layers, requiring testing in the direction parallel and perpendicular to foliation.

For mantle minerals, such as olivine and its high-pressure polymorphs, the β - and γ -spinel wadsleyite and ringwoodite, respectively, Xu et al. (2004) fitted phonon thermal diffusivity measured to 1373 K and 20 GPa to an exponential equation in temperature yielding values for the exponent between $-0.563(35) - -0.793(17)$ suggesting that fitted phonon thermal conductivity varies with $T^{-1/2} - T^{-1}$ (Tab. 5).

Tab. 7 Coefficients for fitting the variation of thermal diffusivity ($10^{-6} \text{ m}^2 \text{ s}^{-1}$) with temperature (K) according to eq. (32); Fo: forsterite; FoCo: Co-doped forsterite (Pertermann & Hofmeister, 2006).

Sample	Chemical Composition	$a \times 10^6$ ($\text{m}^2 \text{ s}^{-1}$)	$b \times 10^6$ ($\text{m}^2 \text{ s}^{-1} \text{ K}$)	$c \times 10^6$ ($\text{m}^2 \text{ s}^{-1} \text{ K}^2$)	T_{max} (°C)	
<i>single crystals</i>						
olivines	Fo[001]	Mg_2SiO_4	0.3081	679.6	213492	985
	FoCo[001]	$\text{Mg}_{1.99}\text{Co}_{0.01}\text{SiO}_4$	0.2347	587.8	172482	1477
	[010]	„	0.2415	115.4	165515	1181
	Needles[100]	$\text{Mg}_{1.84}\text{Fe}_{0.16}\text{SiO}_4$	0.7088	57.7	202533	985
	[010]	„	0.3100	100.6	86470	739
	[001]	„	0.3805	381.3	79703	886
sinhalite	Sumput[010]	$\text{Mg}_{1.87}\text{Fe}_{0.13}\text{SiO}_4$	0.3135	127.2	73824	983
	[010]	MgAlBO_4	0.5546	-128.1	432571	741
chrysoberyl	[100]	BeAl_2O_4	0.5366	551.7	566872	990
	[010]	„	0.3516	415.2	388978	989
	[001]	„	0.6371	428.2	543382	990
<i>polycrystalline samples</i>						

Sample		Chemical Composition	$a \times 10^6$ ($m^2 s^{-1}$)	$b \times 10^6$ ($m^2 s^{-1} K$)	$c \times 10^6$ ($m^2 s^{-1} K^2$)	T_{max} ($^{\circ}C$)
dunites	#1	$\sim Mg_{1.8}Fe_{0.2}SiO_4$	0.2291	290.0	92938	888
	#2	"	0.3563	178.4	93356	1083
monticellite-bearing rock		$Ca_{1.15}Mg_{0.79}Mn_{0.06}SiO_4$	0.3816	153.0	23706	985
hortonolite-bearing rock		$Mg_{1.2}Fe_{0.8}SiO_4$	0.2826	301.2	12638	705
fayalite-bearing slag		$\sim Fe_{1.98}Mn_{0.02}SiO_4$	0.2637	83.9	21216	886
fayalite-bearing rock		$\sim Fe_{1.84}Mn_{0.02}Mg_{0.14}SiO_4$	0.1798	265.3	15688	887

Pertermann & Hofmeister (2006) measured thermal diffusivity on oriented single crystals and polycrystalline samples of olivine-group minerals with the laser-flash method at temperatures of up to about 1500 °C. They fitted the data to a second order polynomial in T:

$$\kappa_p(T) = a + b/T + c/T^2 \quad (T \text{ in K}). \quad (32)$$

Values for the coefficients a, b, and c fitted to data measured on single crystal and polycrystalline samples are shown in Tab. 7.

Osako et al. (2004) fitted thermal diffusivity measured to 1100 K and 8.3 GPa on isotropic, single-crystal garnet and anisotropic olivine ($Fe_{0.93}Fa_{0.07}$; in three crystallographic directions) as upper and lower mantle constituents, respectively, to a linear equation in inverse temperature. (Tab. 6). They found a strong anisotropy in olivine which they assume to prevail throughout the olivine stability field in the mantle down to 410 km.

Variation with pressure

Tommasi et al. (2001) measured thermal diffusivity in the crystallographic [100] and [010] directions parallel and perpendicular to a strain-induced foliation, respectively, as a function of temperature at atmospheric pressure on spinel lherzolites and spinel harzburgite. These rocks are considered representative for the sub-continental and sub-oceanic mantle, respectively. They found an anisotropy in thermal diffusivity on the order of 25 % with the maximum aligned in the direction of strain. Support of their experimental findings was provided by corroborating petrophysical modeling.

For mantle minerals, such as olivine and its high-pressure polymorphs, the β - and γ -spinel wadsleyite and ringwoodite, respectively, Xu et al. (2004) fitted phonon thermal diffusivity measured to 1373 K and 20 GPa to a linear equation in pressure yielding a pressure coefficient of 0.036(4) GPa^{-1} (Tab. 5).

Osako et al. (2004) fitted thermal diffusivity measured to 1100 K and 8.3 GPa on isotropic, single-crystal garnet and anisotropic olivine ($Fe_{0.93}Fa_{0.07}$; in three crystallographic directions) as upper and lower mantle constituents, respectively, to an exponential equation in pressure (Tab. 6). The pressure dependence of garnet and olivine was found to be on the order of 4 % GPa^{-1} – 5 % GPa^{-1} and 3 % GPa^{-1} – 4 % GPa^{-1} , respectively.

Variation with other factors

Micro-cracks and grain boundaries give rise to increased thermal resistance and to a reduction of the mean free path of radiation due to scattering of radiation. It is somewhat debated below which grain size the effect is negligible: Based on the agreement between diffusivities measured on minerals and rocks, Gibert et al. (2003) concluded that the effect of grain boundaries, thermal cracking, and secondary phases is negligible. Along the same lines, Seipold (1998)

argued that grain size is much larger than the phonon mean free path and therefore grain boundaries should not interfere with heat diffusion. Branlund & Hofmeister (2008) confirm this for quartzites, but find diffusivities measured on chert, agate, and chalcedony to be lowered by grain boundaries. They propose that grain sizes above 1 μm should not affect heat transfer.

Additional advective heat transfer was identified by Seipold & Schilling (2003) due to the release of water adsorbed at the inner surfaces of voids (i. e. pores and cracks) in rocks at about 450 K and by dehydration of serpentinite at 850 K. Both processes create high local overpressures which are relieved by cracking if the overpressure exceeds the tensile strength of the rock. The resulting flow is then accompanied by a corresponding advective heat transfer. This phenomenon was observed and studied in laboratory experiments (Seipold & Schilling, 2003) but has implications for the lower crust and upper mantle with respect to recrystallization processes involving the discharge of fluids. These “crustal burps” provide the only conceivable way how some fluids from the mantle or lower crust may find their way to the Earth’s surface. The example discussed by Seipold & Schilling, (2003) involves liberating water of crystallization during the conversion of serpentinite into forsterite and talc, followed by the formation of enstatite. As this involves heat advection as a separate heat transfer mechanism, this process is better addressed separately and not parameterized into some sort of “effective” heat transport property not directly linked to a physical process.

Summary

Understanding the thermal regime of the Earth requires appreciation of properties and mechanisms for storage, transport, and generation of heat with the Earth. Both experimental and indirect methods are available for inferring the corresponding rock properties. Steady-state heat conduction or transient heat diffusion is the dominant transport process in the Earth’s crust, except when appreciable fluid flow provides a mechanism for heat advection. For most crustal and mantle rocks, heat radiation sets in at temperatures above about 450 °C and becomes significant only at temperatures above 1200 °C. At temperatures above 2500 °C heat radiation becomes a dominant mechanism.

Acknowledgment

Extensive and constructive comments provided by an anonymous reviewer are greatly appreciated. Dr. Sukanta Roy kindly helped to meet the size limit of this contribution.

Bibliography

- Aronsson, J. R., Bellotti, L. H., Eckroad, S. W., Emslie, A. G., McConnell, R. K., von Thüna, P. C., 1970. Infrared Spectra and Radiative Thermal Conductivity of Minerals at High Temperatures, *J. Geophys. Res.*, 75(17), 3443-3456.
- Beardmore, G. R., Cull, J. P., 2001. *Crustal Heat Flow*, University Press, Cambridge.
- Beck, A. E., 1988. Methods for determining thermal conductivity and thermal diffusivity, In: R. Hänel, L. Rybach, L. Stegena (eds.), *Handbook of Terrestrial Heat Flow Density Determination*, Kluwer, Dordrecht, pp. 87-124.

- Berman, R. G., 1988. Internally-Consistent Thermodynamic Data for Minerals in the System Na₂O-K₂O-CaO-MgO-FeO-Fe₂O₃-Al₂O₃-SiO₂-TiO₂-H₂O-CO₂, *J. Petrol.*, 29(2), 445-522.
- Birch, F., 1942. Thermal conductivity and diffusivity, In: F. Birch, J. F. Schairer, H. C. Spicer (eds.), *Handbook of Physical Constants*, Special Paper 36, Geological Soc. of America, New York, pp. 243-266.
- Blumm, J., Lemarchand, S., 2002. Influence of test conditions on the accuracy of laser flash measurements, *High Temp.-High Pres.*, 34, 523-528.
- Branlund, J. M., Hofmeister, A. M., 2008. Factors affecting heat transfer in natural SiO₂ solids, *Am. Mineralogist*, 93, 1620-1629.
- Bruggeman, D. A. G., 1935. Berechnung verschiedener Konstanten von heterogenen Substanzen - I. Dielektrizitätskonstanten und Leitfähigkeiten der Mischkörper aus isotropen Substanzen, *Ann. d. Physik*, 24, 636-679.
- Buntebarth, G., 1991. Thermal properties of the KTB-Oberpfalz VB core samples at elevated temperature and pressure, *Scientific Drilling* 2, 73-80.
- Buntebarth, G., Schopper, J. R., 1998. Experimental and theoretical investigations on the influence of fluids, solids and interactions between them on thermal properties of porous rocks, *Physics and Chemistry of the Earth*, 23, 1141-1146.
- Carmichael, R. S. (ed.), 1984. *CRC Handbook of Physical Properties of Rocks III*, CRC Press, Boca Raton FL.
- Čermák, V., Rybach, L., 1982. Thermal Conductivity and Specific Heat of Minerals and Rocks, In: G. Angenheister (ed.), *Landolt-Börnstein: Numerical Data and Functional Relationships in Science and Technology*, New Series, V(1a), Springer, Berlin, pp. 305-343.
- Clark Jr., S. P., 1957. Radiative transfer in the Earth's mantle, *EOS Trans. Am. Geophys. Union*, 38, 931-938.
- Clark Jr., S. P., 1966. Thermal Conductivity, In: S. P. Clark Jr. (ed.), *Handbook of Physical Constants*, Memoir 97, Geol. Soc. of America, New York, pp. 459-482.
- Clark Jr., S. P., 1969. Heat Conductivity in the Mantle, In: P. J. Hart (ed.), *The Earth's Crust and Upper Mantle*, Geophysical Monograph 13, Am. Geophys. Union, Washington D.C., pp. 622-626.
- Clauser, C., 1988. Opacity - the concept of radiative thermal conductivity, In: R. Hänel, L. Rybach, L. Stegena (eds), *Handbook of Terrestrial Heat Flow Density Determination*, Kluwer, Dordrecht, pp. 143-165.
- Clauser, C., 2006. Geothermal Energy, In: K. Heinloth (ed.), *Landolt-Börnstein, Group VIII: Advanced Materials and Technologies, Vol. 3 Energy Technologies, Subvol. C: Renewable Energies*, Springer, Heidelberg-Berlin, pp. 480-595.
- Clauser, C., 2009. Heat Transport Processes in the Earth's Crust, *Surveys in Geophysics*, 30, 163-191, doi: 10.1007/s10712-009-9058-2.
- Clauser, C., Huenges, E., 1995. Thermal Conductivity of Rocks and Minerals. In: T. J. Ahrens (ed.), *Rock Physics and Phase Relations - a Handbook of Physical Constants, AGU Reference Shelf, Vol. 3*, pp. 105-126, American Geophysical Union, Washington.
- Crain, E. R., 1986. *The Log Analysis Handbook*, Quantitative Log Analysis Methods Series, Vol. 1, Pennwell Publishing, Tulsa, OK.

- Davis, E. E., 1988. Oceanic heat-flow density, In: R. Hänel, L. Rybach, L. Stegena (eds.), *Handbook of Terrestrial Heat Flow Density Determination*, Kluwer, Dordrecht, pp. 223-260.
- Davis, G. M., Chapman, D. S., Van Wagoner, T. M., Armstrong, P. A., 2007. Thermal conductivity anisotropy of metasedimentary and igneous rocks, *J. Geophys. Res.*, 112(B05216), doi: 10.1029/2006JB004755.
- Debye, P., 1914. Zustandsgleichung und Quantenhypothese mit einem Anhang über Wärmeleitung, In *Vorträge über die kinetische Theorie der Materie und der Elektrizität, Mathematische Vorlesungen an der Universität Göttingen*, VI., Teubner, Leipzig.
- Diment, W. H., Pratt, H. R., 1988. *Thermal Conductivity of Some Rock-Forming Minerals: a Tabulation*, Open File Report 88-690, U. S. Geol. Survey, Denver CO.
- Dreyer, W., 1974. *Materialverhalten anisotroper Festkörper: Thermische und elektrische Eigenschaften*, Springer, Wien.
- Eucken, A., 1911. Über die Temperaturabhängigkeit der Wärmeleitfähigkeit fester Nichtmetalle, *Annalen der Physik*, 4. Folge, 34(2), 185-220.
- Fricke, H., 1924. A mathematical treatment of the electric conductivity and capacity of disperse systems. *Phys. Rev.*, 24, 575-587.
- Gibert, B., Seipold, U., Tommasi, A., Mainprice, D., 2003. Thermal diffusivity of upper mantle rocks: influence of temperature, pressure, and the deformation fabric, *J. Geophys. Res.*, 108(B8), 2359, doi: 10.1029/2002JB002108.
- Goutorbe, B., Lucazeau, F., Bonneville, A., 2006. Using neural networks to predict thermal conductivity from geophysical well logs, *Geophys. J. Int.*, 166(1), 115, doi:10.1111/j.1365-246X.2006.02924.x.
- Hartmann, A., Rath, V., Clauser, C., 2005. Thermal Conductivity from Core and Well log Data, *Int. J. Rock Mech. Mining Sci.*, 42, 1042-1055, doi: 10.1016/j.ijrmms.2005.05.015.
- Hashin, Z., Shtrikman, S., 1962. A variational approach to the theory of the effective magnetic permeability of multiphase materials *J. Appl. Phys.* 33(10), 3125-3131.
- Höfer, M., Schilling, F. R., 2002. Heat transfer in quartz, orthoclase, and sanidine at elevated temperature, *Phys. Chem. Minerals*, 29, 571-584.
- Hofmeister, A. M., 1999. Mantle Values of Thermal Conductivity and the Geotherm from Phonon Lifetimes, *Science*, 283, 1699-1706.
- Hofmeister, A. M., 2005. Dependence of diffusive radiative transfer on grain-size, temperature, and Fe-content: Implications for mantle processes *J. Geodynamics*, 40, 51-72.
- Hofmeister, A. M., 2006. Thermal diffusivity of garnets at high temperature, *Physics and Chemistry of Minerals*, 33, 45-62.
- Hofmeister, A. M., Branlund, J. M., Pertermann, M., 2009. Properties of rocks and minerals - thermal conductivity of the Earth, In: G. D. Price (ed.), *Mineral Physics, Treatise on Geophysics*, Vol. 2, Elsevier, Amsterdam, pp. 543-577.
- Horai, K., Simmons, G., 1969. Thermal conductivity of rock-forming minerals, *Earth Planet. Sci. Lett.*, 6(5), 359-368.
- Horai, K., 1971. Thermal Conductivity of Rock-Forming Minerals, *J. Geophys. Res.*, 76(5), 1278-1308.

- Horai, K., 1991. Thermal Conductivity of Hawaiian Basalt: A New Interpretation of Robertson and Peck's Data, *J. Geophys. Res.*, 96(B3), 4125-4132.
- Kappelmeyer, O., Haenel, R., 1974. *Geothermics - with special reference to application*, Bornträger, Berlin-Stuttgart.
- Kobolev, V. P., Kutas, R. I., Popov, Y. A., 1990. Method and results of research of thermal properties of Ural region rocks with laser scanning, *Geophysical J.*, 12(4), Naukova Dumka, Kiev, 29-37 (in Ukrainian).
- Korvin, G., 1978. The hierarchy of velocity formulae: Generalized mean value theorems, *Acta Geodaetica, Geophysica et Montanista*, 13, 211-222.
- Korvin, G., 1982. Axiomatic characterization of the general mixture rule, *Geoexploration*, 19, 267-276.
- Mottaghy, D. C., Schellschmidt, R., Popov, Y. A., Clauser, C., Kukkonen, I. T., Nover, G., Milanovsky, S., Romushkevich, R. A., 2005. New heat flow data from the immediate vicinity of the Kola super-deep borehole: Vertical variation in heat flow confirmed and attributed to advection, *Tectonophysics*, 401/1-2, 119-142, doi: 10.1016/j.tecto.2005.03.005.
- Osako, M., Ito, E., Yoneda, A., 2004. Simultaneous measurement of thermal conductivity and thermal diffusivity for garnet and olivine under high pressure, *Phys. Earth Planet. Int.*, 143-144, 311-320.
- Parker, W. J., Jenkins, R. J., Butler, C. P., Abbott, G. I., 1961. Flash method of determining thermal diffusivity, heat capacity, and thermal conductivity, *J. Appl. Phys.*, 32(9), 1679-1684.
- Peierls, R., 1929. Zur kinetischen Theorie der Wärmeleitung in Kristallen, *Annalen der Physik*, 5. Folge, 3, 1055-1101.
- Pertermann, M., Hofmeister, A. M., 2006. Thermal diffusivity of olivine-group minerals at high temperature, *Am. Mineralogist*, 91, 1747-1760.
- Petrudin, G. I., Popov, V. G., Il'in, I. A., 2004. Conductive heat Transfer in Plagioclases, *Izvestiya, Physics of the Solid Earth (English Translation)*, 40(9), 752-759.
- Popov, Y. A., Berezin, V. V., Solov'yev, G. A., Romushkevich, R. A., Korostelev, V. M., Kostyurin, A. A., Kulikov, I. V., 1987. Thermal conductivity of minerals, *Izvestiya, Physics of the Solid Earth (English Translation)*, 23(3), 245-253.
- Popov, Y. A., Mandel, A. M., 1998. Geothermal study of anisotropic rock masses, *Izvestiya, Physics of the Solid Earth (English Translation)*, 34(11), 903-915.
- Popov, Y. A., Pevzner, L. A., Romushkevich, R. A., Korostelev, V. M., Vorob'ev, M. G., 1995. Thermophysical and geothermal sections obtained from Kolvinskaya well logging data, *Izvestiya, Physics of the Solid Earth (English Translation)*, 30(9), 778-789.
- Popov, Y. A., Pevzner, L. A., Pimenov, V. P., Romushkevich, R. A., 1999a. New geothermal data from the Kola superdeep well SG-3, *Tectonophysics*, 306(3-4), 345-366.
- Popov, Y. A., Pribnow, D. F. C., Sass, J. H., Williams, C. F., Burkhardt, H., 1999b. Characterization of rock thermal conductivity by high-resolution optical scanning, *Geothermics*, 28, 253-276.

- Popov, Y., Tertychnyi, V., Romushkevich, R., Korobkov, D., Pohl, J., 2003. Interrelations between thermal conductivity and other physical properties of rocks: Experimental data, *Pure and Applied Geophysics*, 160, 1137-1161.
- Ray, L., Förster, H.-J., Schilling, F. R., Förster, A., 2006. Thermal diffusivity of felsic to mafic granulites at elevated temperatures, *Earth Planet. Sci. Lett.*, 251, 241-253.
- Reibelt, M., 1991. *Study on the influence of surface structure and fluid saturation of rocks on the determination of thermal conductivity by a half-space line source*, Diploma thesis (unpublished; in German), Institut für Angewandte Geophysik, Petrologie und Lagerstättenforschung, Technische Universität Berlin, Germany.
- Roy, R. F., Beck, A. E., Touloukian, Y. S., 1981. *Thermophysical Properties of Rocks*, In: Y. S. Touloukian, W. R. Judd, R. F. Roy (eds.), *Physical Properties of Rocks and Minerals*, McGraw-Hill/CINDAS Data Series on Material Properties, Vol. II-2, McGraw-Hill, New York NY, pp. 409-502.
- Rosseland, S., 1930. The principles of quantum theory, In: G. Eberhard, A. Kohlschütter und H. Ludendorff (eds.), *Handbuch der Astrophysik*, 3(1), Springer, Berlin, pp. 452-474.
- Sass, J. H., Lachenbruch, A. H., Moses Jr., T. H., Morgan, T., 1992. Heat flow from a scientific research well at Cajon Pass, California, *J. Geophys. Res.* 97(B4), 5017-5030.
- Schärmeli, G., 1982. Anisotropy of olivine thermal conductivity at 2.5 GPa up to 1500 K measured on optically non-thick sample, In: W. Schreyer (ed.), *High-Pressure Researches in Geoscience*, Schweizerbart, Stuttgart, Germany, pp. 349-373.
- Schilling, F. R., 1999. A transient technique to measure thermal diffusivity at elevated temperatures, *Eur. J. Mineral.*, 11, 1115-1124.
- Schulz, B., 1981. Thermal conductivity of porous and highly porous materials, *High Temp.-High Pres.*, 13, 649-660.
- Seipold, U., 1998. Temperature dependence of thermal transport properties of crystalline rocks - a general law, *Tectonophysics*, 291(1-4), 161-171.
- Seipold, U., Schilling, R. R., 2003. Heat transport in serpentinites, *Tectonophysics*, 370, 147-162.
- Shankland, T. J., Nitsan, U., Duba, A. G., 1979. Optical absorption and radiative heat transport in olivine at high temperature, *J. Geophys. Res.*, 84(B4), 1603-1610.
- Somerton, W. H., 1992. *Thermal Properties and Temperature Related Behavior of Rock/Fluid Systems*, Elsevier, Amsterdam.
- Tommasi, A., Gibert, B., Seipold, U., Mainprice, D., 2001. Anisotropy of thermal diffusivity in the upper mantle, *Nature*, 411, 783-786.
- Vosteen, H.-D., Schellschmidt, R., 2003. Influence of temperature on thermal conductivity, thermal capacity, and thermal diffusivity for different types of rock *Physics and Chemistry of the Earth*, 28(9-11), 499-509.
- Whittington, A. G., Hofmeister, A. M., Nabelek, P. I., 2009. Temperature-dependent thermal diffusivity of the Earth's crust and implications for magmatism, *Nature*, 458, 319-321, doi: 10.1038/nature07818.

- Williams, C. F., Anderson, R. A., 1990. Thermophysical Properties of the Earth's Crust: In Situ Measurements From Continental and Ocean Drilling, *J. Geophys. Res.*, 95(B6), 9209-9236.
- Xu, Y., Shankland, T. J., Linhardt, S., Rubie, D. C., Langenhorst, F., Klasinski, K., 2004. Thermal diffusivity and conductivity of olivine, wadsleyite and ringwoodite to 20 GPa and 1373 K, *Phys. Earth Planet. Int.*, 143-144, 321-336.
- Zimmerman, R. W., 1984. *The effect of pore structure on the pore and bulk compressibilities of consolidated sandstones*, Ph.D. thesis, University of California, Berkeley, Ca..
- Zimmerman, R. W., 1989. Thermal conductivity of fluid-saturated rocks, *J. Petrol. Sci. Eng.*, 3(3), 219-227.
- Zoth, G., Hänel, R., 1988. Appendix, In: R. Hänel, L. Rybach, L. Stegena (eds.), *Handbook of Terrestrial Heat Flow Density Determination*, Kluwer Academic Publishers, Dordrecht, pp. 449-466.

Cross-references

Thermal Storage and Transport Properties of Rocks, 2: Thermal Conductivity and Diffusivity
Heat flow (continental, oceanic)
Geothermal record of climate change
Continental Lithosphere, Thermal Structure

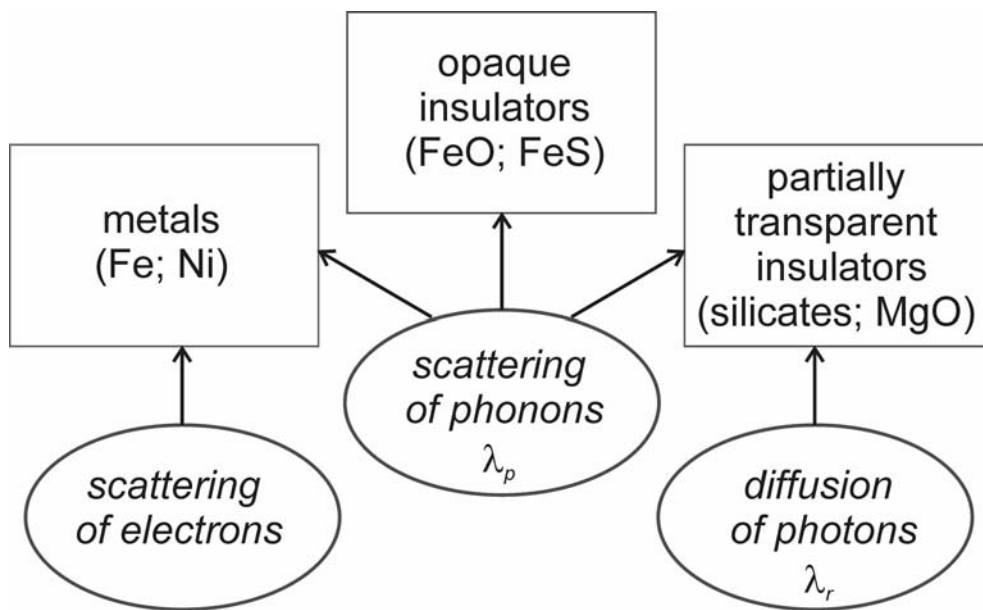


Fig. 1 Different types of material in the Earth and associated mechanisms of heat transport (redrawn after Hofmeister et al., 2009).

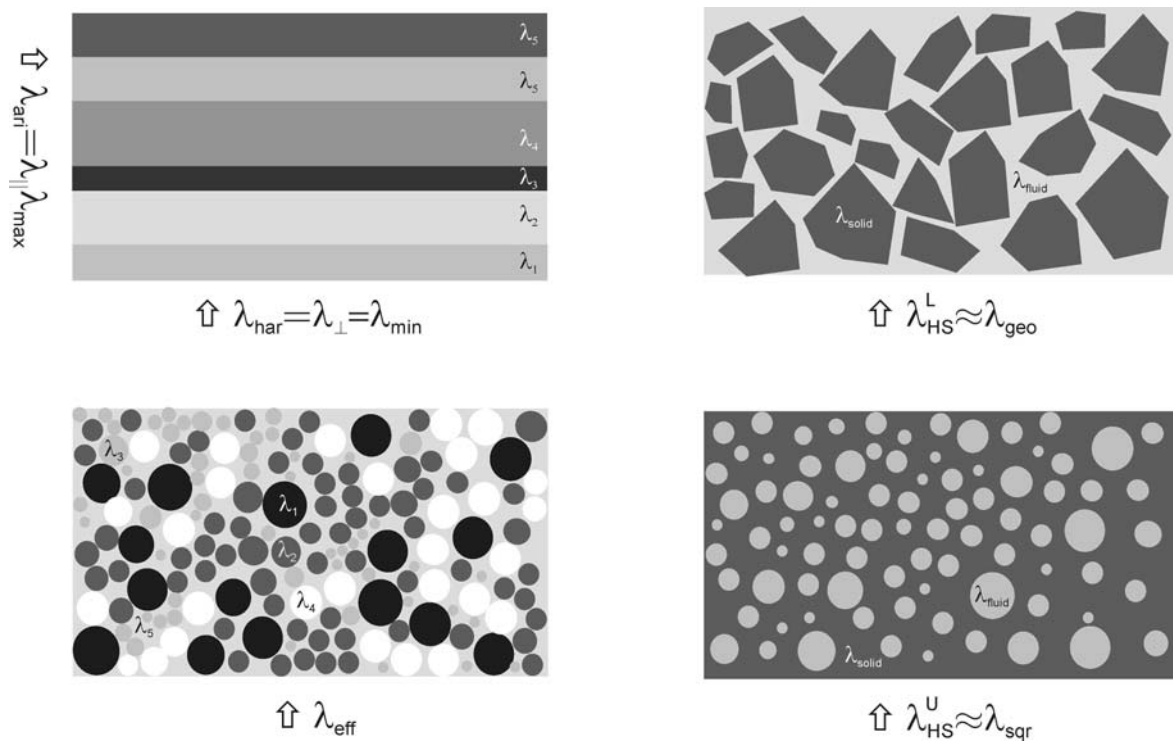


Fig. 2 Geometrical arrangement of layers, mineral grains, and pores assumed in different models for calculating mean bulk thermal conductivity of a composite medium: arithmetic (λ_{ari}), harmonic (λ_{har}), geometric (λ_{geo}), square root (λ_{sqr}), Hashin-Shtrikman upper (λ_{HS}^U) and lower (λ_{HS}^L) bounds, and effective medium (λ_{eff}).

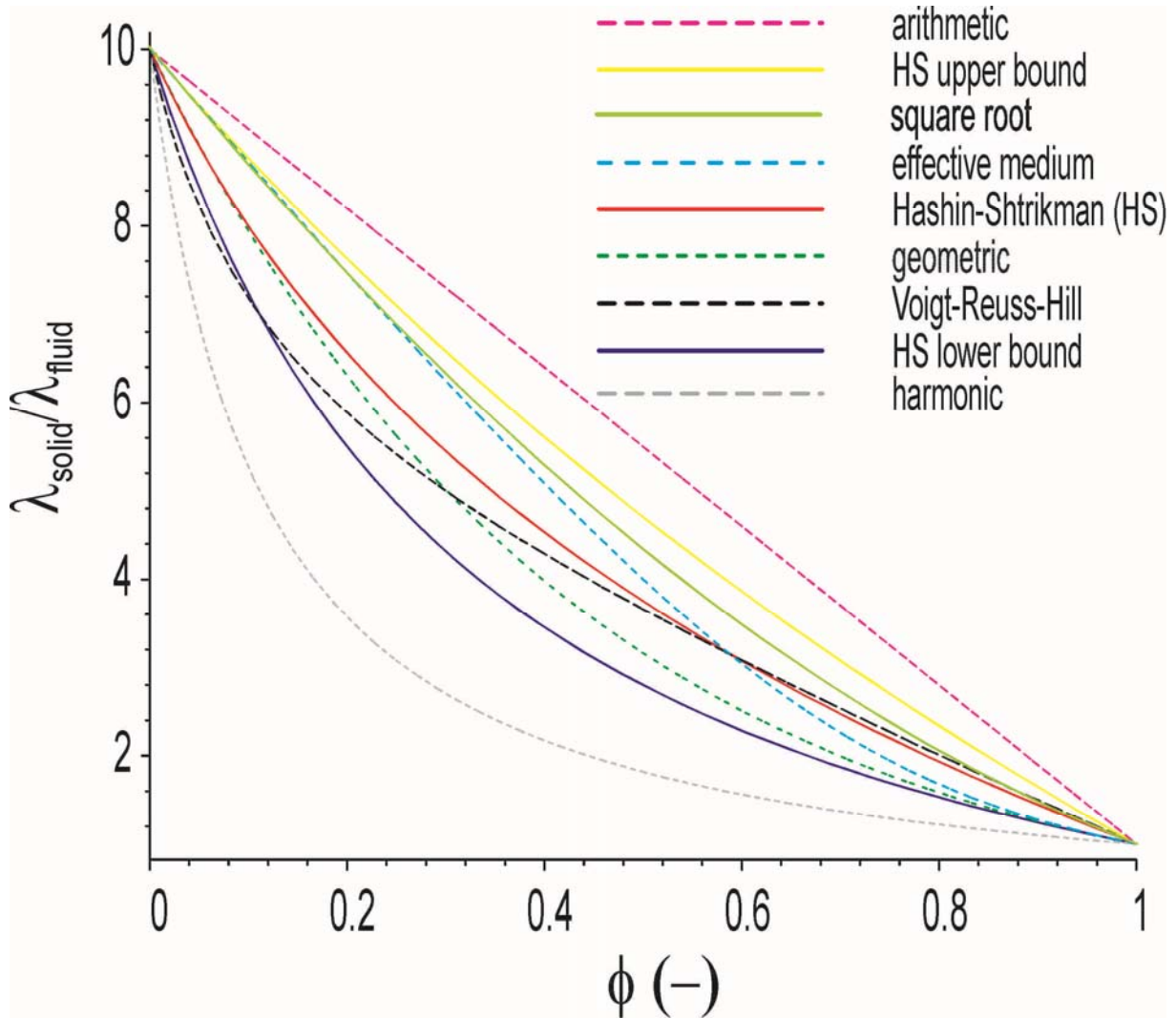


Fig. 3 Variation of thermal conductivity λ of a two-phase rock with porosity ϕ according to the means in eqs. (2) – (5) for solid and fluid thermal conductivities of $\lambda_{\text{solid}}=6 \text{ W m}^{-1} \text{ K}^{-1}$ and $\lambda_{\text{fluid}} = 0.6 \text{ W m}^{-1} \text{ K}^{-1}$, respectively: arithmetic (λ_{ari}); Hashin-Shtrikman upper bound ($\lambda_{\text{HS}}^{\text{U}}$); square root (λ_{sqr}); effective medium (λ_{eff}); Hashin-Shtrikman (λ_{HS}); geometric (λ_{geo}); Voigt-Reuss-Hill average (λ_{VRH}); Hashin-Shtrikman lower bound ($\lambda_{\text{HS}}^{\text{L}}$); harmonic (λ_{har}).

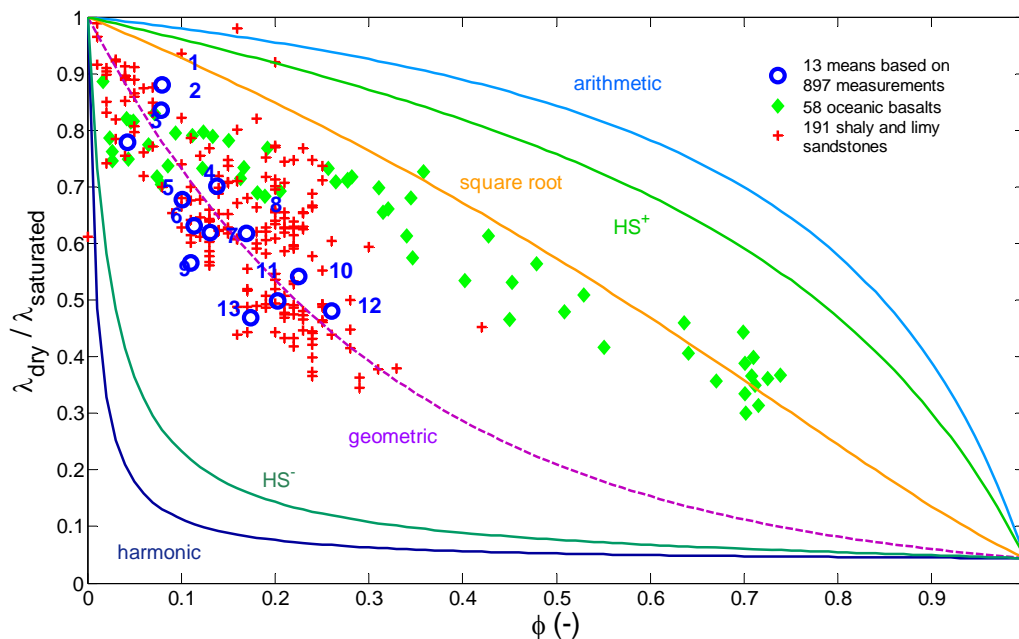


Fig. 4 Variation of thermal conductivity ratio $\lambda_{\text{dry}}/\lambda_{\text{sat}}$ (measured in dry and saturated condition) with porosity ϕ for different rock types. Numbered open circles represent means based on measurements on 897 sedimentary rock samples (Kobolev et al., 1990; Popov et al., 1995; 1999a; see also Clauser, 2006): (1) 21 limestones; (2) 54 lime-stones; (3) 13 quartz sandstones; (4) 44 quartz silt-stones; (5) 35 conglomerates; (6) 141 quartz sandstones; (7) 33 claystones; (8) 99 polymictic sandstones; (9) 30 quartz sandstones; (10) 22 claystones; (11) 65 quartz silt-stones; (12) 99 quartz silt-stones; (13) 241 quartz silt-stones. Shown for comparison are data measured on 58 oceanic basalts (diamonds) and 191 shaly and limy sandstones (crosses). Curves labeled arithmetic, HS^+ , square root, geometric, HS^- , and harmonic, correspond to the arithmetic, upper Hashin-Shtrikman, square root, geometric, lower Hashin-Shtrikman, and harmonic mixing laws, λ_{ari} , $\lambda_{\text{HS}}^{\text{U}}$, λ_{sqr} , λ_{geo} , $\lambda_{\text{HS}}^{\text{L}}$, and λ_{har} , respectively (eqs. (27) – (29)) (Clauser, 2006).

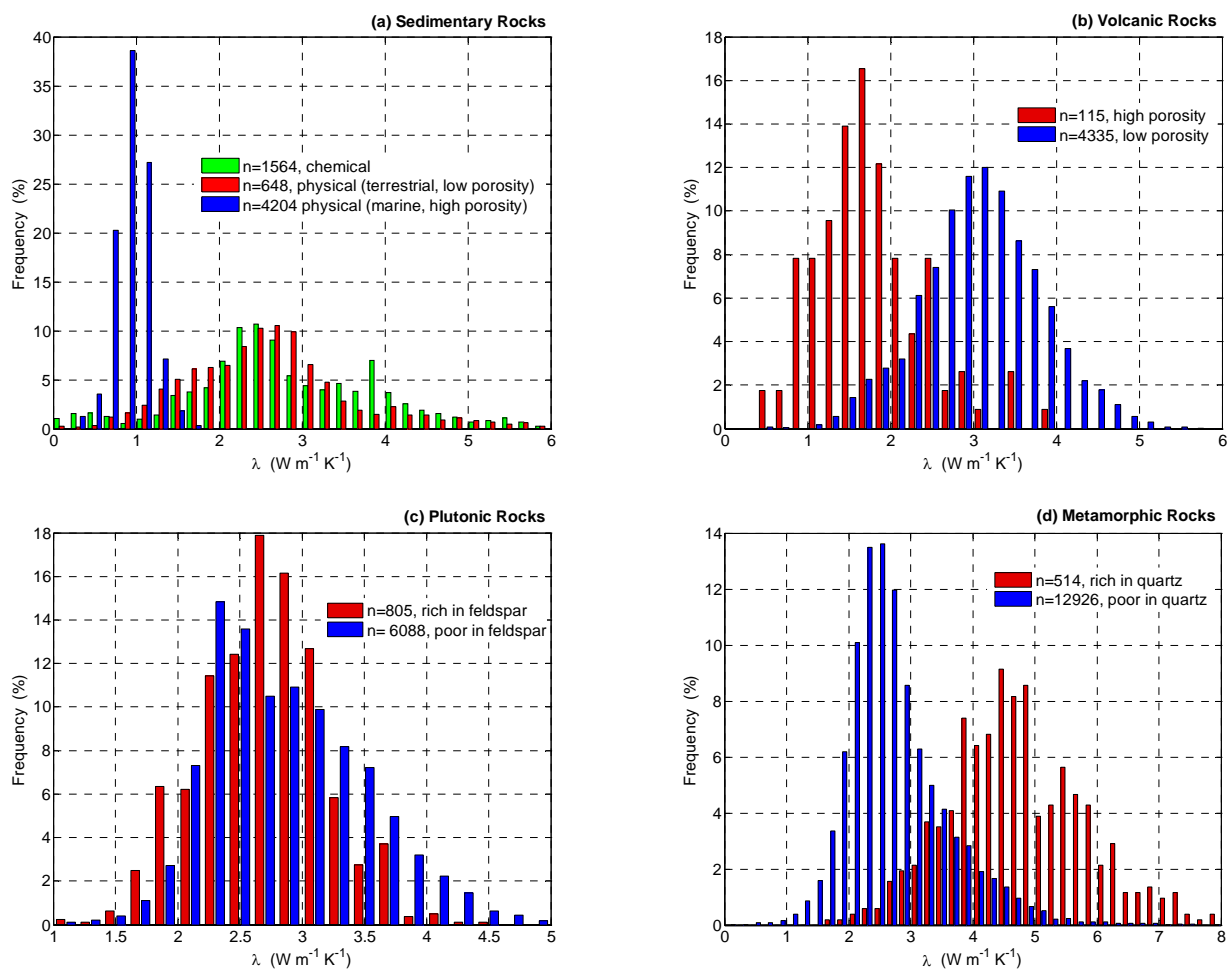


Fig. 5 Histograms of thermal conductivity for (a) sedimentary, (b) volcanic, (c) plutonic, and (d) metamorphic rocks (Clauser, 2009).

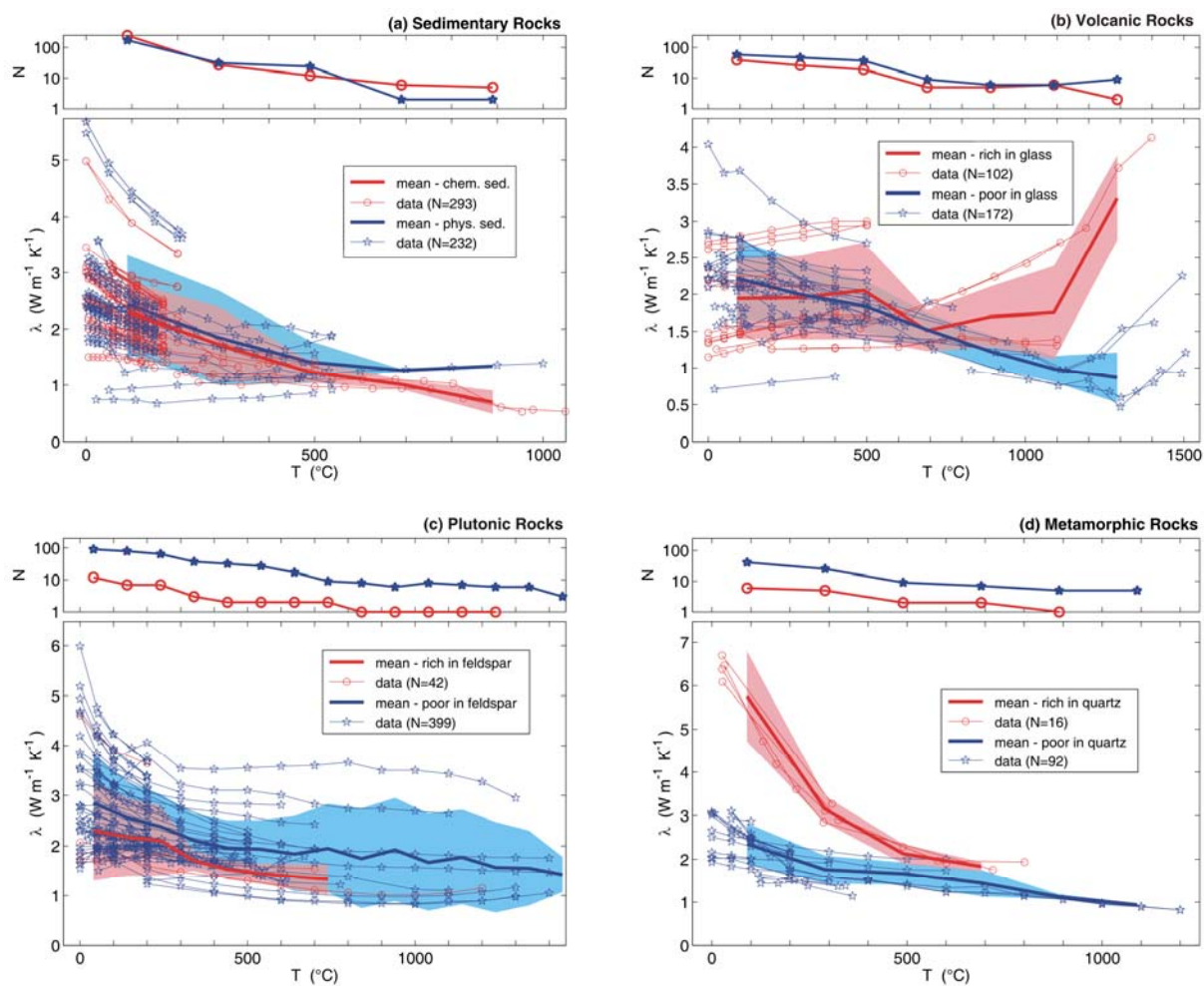


Fig. 6 Variation of thermal conductivity with temperature for (a) sedimentary, (b) volcanic, (c) plutonic, and (d) metamorphic rocks. Color shading indicates a range defined by plus and minus one standard deviation and N is the number of data at each temperature (Clauser, 2009).

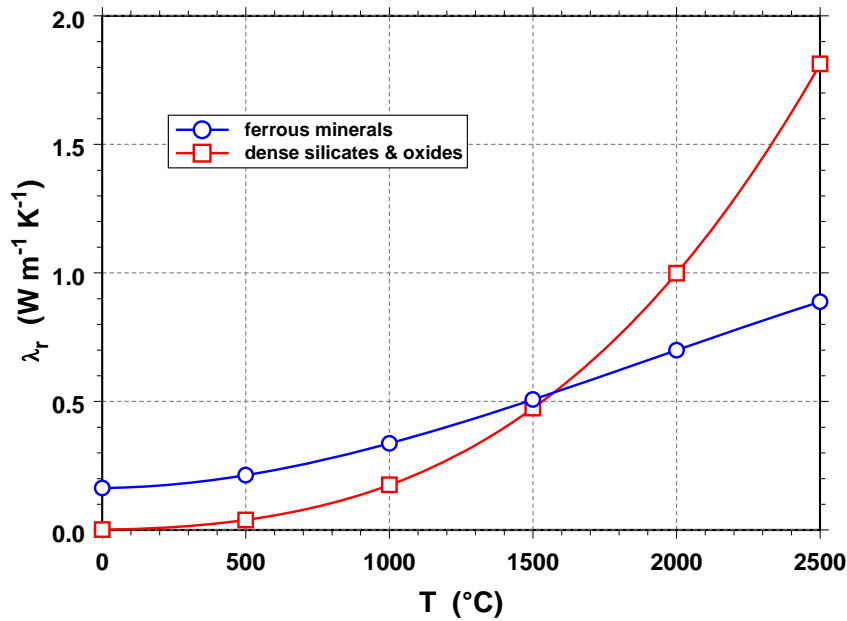


Fig. 7 Variation of radiative thermal conductivity λ_r of ferrous minerals, dense silicates, and oxides with temperature according to eq. (27) (Hofmeister, 1999).

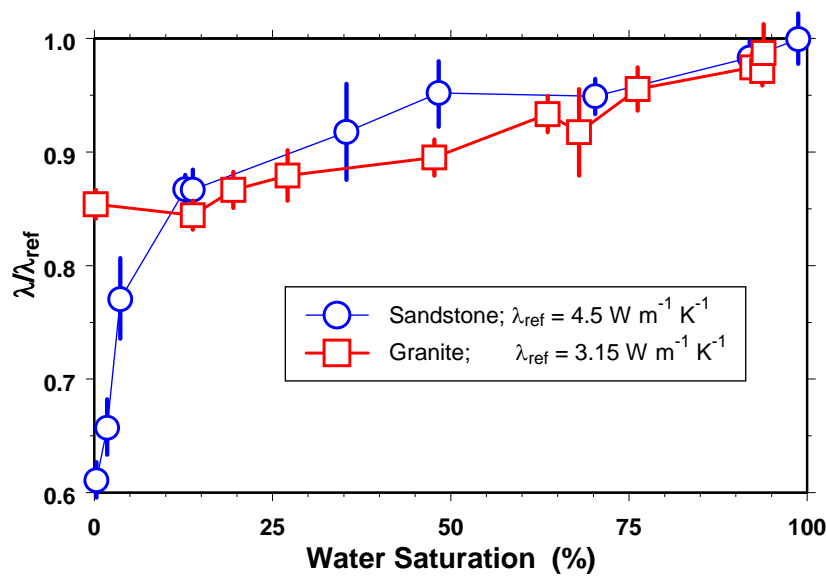


Fig. 8 Variation of thermal conductivity with partial saturation for a sandstone (circles; $\phi = 18\%$) and granite (squares; $\phi = 1\%$) saturated with water and standard deviations (bars); values normalized by reference thermal conductivities shown in legend (Clauser (2006) based on data of Reibelt (1991)).